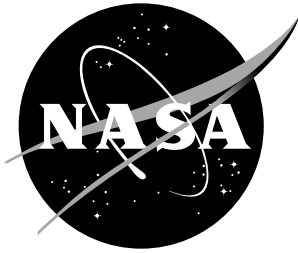


NASA / CR-97-206259



# Radar Reflectivity in Wingtip-Generated Wake Vortices

*Robert E. Marshall, Ashok Mudukutore, and Vicki L. H. Wissel*

---

December 1997

## *The NASA STI Program Office ... in Profile*

Since its founding, NASA has been dedicated to the advancement of aeronautics and space science. The NASA Scientific and Technical Information (STI) Program Office plays a key part in helping NASA maintain this important role.

The NASA STI Program Office is operated by Langley Research Center, the lead center for NASA's scientific and technical information. The NASA STI Program Office provides access to the NASA STI Database, the largest collection of aeronautical and space science STI in the world. The Program Office is also NASA's institutional mechanism for disseminating the results of its research and development activities. These results are published by NASA in the NASA STI Report Series, which includes the following report types:

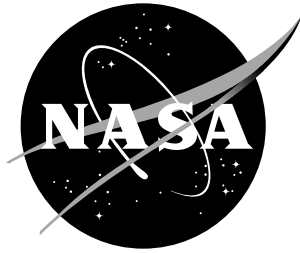
- **TECHNICAL PUBLICATION.** Reports of completed research or a major significant phase of research that present the results of NASA programs and include extensive data or theoretical analysis. Includes compilations of significant scientific and technical data and information deemed to be of continuing reference value. NASA counter-part of peer reviewed formal professional papers, but having less stringent limitations on manuscript length and extent of graphic presentations.
- **TECHNICAL MEMORANDUM.** Scientific and technical findings that are preliminary or of specialized interest, e.g., quick release reports, working papers, and bibliographies that contain minimal annotation. Does not contain extensive analysis.
- **CONTRACTOR REPORT.** Scientific and technical findings by NASA-sponsored contractors and grantees.
- **CONFERENCE PUBLICATION.** Collected papers from scientific and technical conferences, symposia, seminars, or other meetings sponsored or co-sponsored by NASA.
- **SPECIAL PUBLICATION.** Scientific, technical, or historical information from NASA programs, projects, and missions, often concerned with subjects having substantial public interest.
- **TECHNICAL TRANSLATION.** English-language translations of foreign scientific and technical material pertinent to NASA's mission.

Specialized services that help round out the STI Program Office's diverse offerings include creating custom thesauri, building customized databases, organizing and publishing research results ... even providing videos.

For more information about the NASA STI Program Office, you can:

- Access the NASA STI Program Home Page at <http://www.sti.nasa.gov/STI-homepage.html>
- E-mail your question via the Internet to [help@sti.nasa.gov](mailto:help@sti.nasa.gov)
- Fax your question to the NASA Access Help Desk at (301) 621-0134
- Phone the NASA Access Help Desk at (301) 621-0390
- Write to:  
NASA Access Help Desk  
NASA Center for AeroSpace Information  
800 Elkridge Landing Road  
Linthicum Heights, MD 21090-2934

NASA / CR-97-206259



# Radar Reflectivity in Wingtip-Generated Wake Vortices

*Robert E. Marshall, Ashok Mudukutore, and Vicki L. H. Wissel  
Center for Aerospace Technology, Research Triangle Institute, Hampton, VA*

National Aeronautics and  
Space Administration

Langley Research Center  
Hampton, Virginia 23681-2199

Prepared for Langley Research Center  
under Contract NAS1-18925

---

December 1997

# CONTENTS

LIST OF FIGURES .....	iv
LIST OF TABLES .....	vi
EXECUTIVE SUMMARY .....	vii
1.0 INTRODUCTION .....	1
2.0 TERMINAL AREA SIMULATION SYSTEM (TASS) MODEL OUTPUT FOR CLEAR AIR AND FOG .....	4
2.1 <u>TASS Output for Clear Air</u> .....	4
2.2 <u>TASS Output for Fog</u> .....	8
2.3 <u>TASS Wind Variables</u> .....	10
3.0 RADAR REFLECTIVITY MODEL FOR CLEAR AIR .....	14
3.1 <u>Derived Thermodynamic Variables</u> .....	14
3.2 <u>Refractive Index of the Clear Atmosphere</u> .....	17
3.3 <u>Scales of Turbulence in the Clear Atmosphere</u> .....	20
3.4 <u>Volume Reflectivity in the Clear Atmosphere</u> .....	27
4.0 RADAR REFLECTIVITY MODEL FOR FOG .....	31
4.1 <u>Atlas Radar Reflectivity Factor Model</u> .....	32
4.2 <u>de Wolf Radar Reflectivity Factor Model</u> .....	33
4.3 <u>Comparison of Models and Assumptions</u> .....	34
4.4 <u>Volume Reflectivity in Fog</u> .....	37
5.0 CONCLUSIONS .....	39
REFERENCES .....	41
GLOSSARY .....	43

## LIST OF FIGURES

Figure 2–1. Pressure (mb) predicted by TASS in the wake of a C-130 at 30 seconds after rollup. (clear air).....	5
Figure 2–2. Temperature (°K) predicted by TASS in the wake of a C-130 at 30 seconds after rollup. (clear air) .....	6
Figure 2–3. Absolute humidity ( $\text{gm m}^{-3}$ ) predicted by TASS in the wake of a C-130 at 30 seconds after rollup. (clear air).....	7
Figure 2–4. TKE dissipation rate ( $\text{watt kg}^{-1}$ ) predicted by TASS in the wake of a C-130 at 30 seconds after rollup. (clear air).....	8
Figure 2–5. Temperature profile for the averaged VAFB fog layer.....	9
Figure 2–6. Liquid water content profile for the averaged VAFB fog layer.....	9
Figure 2–7. Liquid water content in the wake of a C-130 generated in the averaged VAFB fog layer. (dense advection fog).....	10
Figure 2–8. Horizontal wind speed in the wake of the C-130 at 30 sec after rollup.....	11
Figure 2–9. Vertical wind speed in the wake of the C-130 at 30 sec after rollup. ....	11
Figure 2–10. Vector plot of wind velocity in the C-130 wake at 30 sec after rollup. ....	12
Figure 2–11. Vertical wind speed along a line through the core of the C-130 wake at 30 sec after rollup.....	13
Figure 3–1. Potential temperature (°K) in the wake of a C-130 at 30 seconds after rollup. ..	15
Figure 3–2. Dry air density ( $\text{kg m}^{-3}$ ) in the wake of a C-130 at 30 seconds after rollup.....	16
Figure 3–3. Water vapor mixing ratio ( $\text{kg kg}^{-1}$ ) in the wake of a C-130 at 30 seconds after rollup. ....	17
Figure 3–4. Refractivity in the wake of a C-130 at 30 sec after rollup. ....	19
Figure 3–5. Potential refractive index in the wake of a C-130 at 30 sec after rollup.....	20
Figure 3–7. Schematic representation of a turbulent eddy that is one-half the radar wavelength in diameter. ( $n_1 \equiv$ refractive index inside the eddy; $n_2 \equiv$ refractive index surrounding the eddy).....	21
Figure 3–8. Turbulent Kinetic Energy Spectrum as a function of turbulent eddy wavenumber. ( $d = \lambda/2$ ).....	22
Figure 3–9. Kinematic viscosity in the wake of a C-130 at 30 seconds after rollup.....	24
Figure 3–10. Kolmogorov microscale in the wake of a C-130 at 30 seconds after rollup.....	24
Figure 3–11. The maximum radar frequency based on $5\pi$ times the Kolmogorov microscale in the C-130 wake. ....	25
Figure 3–12. The maximum radar frequency based on the turbulent velocity and mixing length in the C-130 wake. ( $u = 3.9 \text{ m sec}^{-1}$ ; $l = 3.5 \text{ m}$ ).....	27

Figure 3–13. Refractive index structure constant for the C-130 at 30 sec after rollup. ....	30
Figure 4–1. Radar reflectivity factor as calculated from the relationship by Atlas. ( $Z = 0.048 M^2$ ).....	32
Figure 4–2. Radar reflectivity factor in the wake of a C-130, 30 seconds after rollup in the VAFB fog layer using the Atlas empirical relationship. ....	33
Figure 4–3. Radar reflectivity in the wake of a C-130 at 30 seconds after rollup in the VAFB fog layer using the de Wolf empirical relationship between $Z$ and $M$ .....	34
Figure 4–4. Comparison between the Atlas empirical relationship and the analytical relationship for radar reflectivity factor in the VAFB fog layer.....	35
Figure 4–5. Comparison between the de Wolf and Atlas empirical relationship between liquid water content and radar reflectivity factor. ....	36
Figure 4–6. Figure 4–2 minus Figure 4–3 in dB. ....	37
Figure 4–7. Radar volume reflectivity calculated from equation (4.5) and the radar reflectivity factor, $Z$ , from the de Wolf empirical relationship. ....	38

## LIST OF TABLES

Table 2–1. TKE dissipation rates associated with aircraft related levels of turbulence..... 7

## EXECUTIVE SUMMARY

This report documents the first known models for predicting radar reflectivity with resolution smaller than aircraft wingspans in the wakes of aircraft flying in clear air or in fog. The work is part of a broader program within the Sensors Research Branch at the NASA Langley Research Center to design a radar that can locate and quantify wake vortices found in the wakes of commercial aircraft (Marshall, Davis and Caswell, 1997; Marshall and Mudukutore, 1996; and Marshall, Scales and Myers, 1996). A wide range of remote sensing technologies are currently being considered for the NASA Aircraft Vortex Spacing System (AVOSS) to dynamically allocate separation distances for landing aircraft based on the wind and thermodynamic characteristics of the ambient atmosphere and the resulting predictions of wake vortex decay and transport; the remote sensors will verify the predicted vortex behavior and allow for spacing adjustments, as required (Hinton, 1995). In order to define a radar to both locate and quantify individual vortices, a model that quantitatively describes the Doppler radar backscattering characteristics of wake vortices with a grid spacing of less than 10 meters is required.

The radar backscattering characteristics of wake vortices are dependent on the wind, water vapor, liquid water, temperature and pressure of the atmosphere within the wake. These properties are predicted by the NASA Terminal Area Simulation System (TASS) with a resolution of 2 meters or less (Proctor, 1987). These TASS output variables serve as inputs to the wake vortex radar reflectivity models, which predict the radar backscattering properties at each TASS grid point.

In clear air, the wake vortex radar reflectivity model assumes that the radar backscattering mechanism is Bragg Scatter. An ensemble of half radar wavelength wind eddies produced by turbulence within the wake generates half-radar wavelength discontinuities in the refractive index field and provides an efficient backscattering mechanism for radar detection at that wavelength. The TASS output provides the mean refractive index field on a grid of approximately 1 meter; however, turbulence-induced discontinuities in refractive index at the half-radar wavelength are on the order of one centimeter. These discontinuities in refractive index can be quantified using a first-order, turbulence closure technique—eddy diffusivity—which relates the turbulent refractive index characteristics to the gradients of the mean refractive index field obtained from

TASS. The resulting model for radar reflectivity in the wake of an aircraft predicts a coherent structure in the radar reflectivity field. The boundary of the descending volume of air containing the two vortices is marked by a water vapor front, in which radar volume reflectivity is on the order of  $-100 \text{ dB m}^{-1}$ . In the individual vortices, radar volume reflectivity is between  $-120$  and  $-180 \text{ dB m}^{-1}$ .

The turbulence theory used to predict radar reflectivity in clear air assumes that there exists a continuous range of turbulent eddy sizes in which turbulent kinetic energy (TKE) is passed from larger to smaller eddies without energy dissipation in the high Reynolds number wake vortex flow. TKE dissipation occurs at the smaller eddy sizes just outside this non-dissipative, inertial subrange of the TKE eddy wave number spectrum. Radars with half-wavelengths that are equal in diameter to eddies that are in the dissipative range of the TKE eddy wave number spectrum are impractical to develop because they require large antenna gain-transmitter power products to detect the low radar reflectivity from eddies associated with TKE dissipation. The maximum radar frequency appropriate for detection of the wake vortex at each TASS grid point for a practical radar can be predicted by defining the smallest half-radar wavelength turbulent eddies not involved in TKE dissipation. The results of this model indicate that radars between 10 and 30 GHz ( $\lambda \equiv 1 \text{ cm}$ ) may be practical for detecting individual wake vortices, but radars below 10 GHz ( $\lambda \equiv 3 \text{ cm}$ ) are appropriate for detecting the highly reflective boundary of the descending volume of air.

In fog or precipitation where the liquid water drops are small compared to the radar wavelength, the Doppler radar backscattering mechanism is Rayleigh scattering, which results from the electromagnetic interaction of the radar pulse with the liquid water drops. The radar reflectivity factor,  $Z$ , in the wakes of aircraft flying in fog is produced at each TASS grid point by converting liquid water content in fog (TASS output) to  $Z$  using an empirically-derived relationship. Model results show values of  $Z$  vary between  $-20$  and  $-32 \text{ dBZ}$  for aircraft flying in a representative, dense fog layer.

The major conclusions of the report are:

- In clear air, the area of highest radar reflectivity is associated with the boundary of the aircraft wake and not the individual vortices.

- The smallest scales of turbulence are associated with the individual vortices resulting in the potential of using millimeter wave radars to detect individual vortices. These conclusions need to be tested in a variety of clear atmospheres with varying amounts of water vapor.
- A high resolution description of liquid water content facilitates a high resolution prediction of radar reflectivity factor within the wakes of aircraft flying in dense fog.
- As the visibility in fog increases and the liquid water content decreases, a knowledge of the liquid water content distribution by fog drop size may be required for accurate predictions of radar reflectivity factor in the wakes of aircraft flying in fog.

## 1.0 INTRODUCTION

An objective of the NASA Aircraft Vortex Separation System (AVOSS) is to increase the terminal area productivity of airports by reducing the wake vortex separation distance imposed on landing aircraft (Hinton, 1995). The purpose of AVOSS is to dynamically adjust the separation distance between aircraft by predicting the transport and decay characteristics of wake vortices that are generated by the landing aircraft. The transport and decay of wake vortices is primarily dependent on the dynamics and stability of the atmosphere in which they are generated, and AVOSS will provide the dynamic spacing criteria based on real-time meteorological data. In order to validate the predictions made by AVOSS, a remote sensing system that has the ability to locate and quantify wake vortices will provide a “cross-check” of the wake vortex behavior in clear air as well as low visibility atmospheres.

Two remote sensors—Light Detection and Ranging (Lidar) and conventional radar—are being considered as sources of the empirical data with which to validate the analytical model in AVOSS. This report presents the first radar reflectivity models for the wakes of aircraft flying in clear air and fog. These models have been used to assess the performance of a radar design under consideration for use by AVOSS (Marshall and Mudukutore, 1996; and Marshall, et. al, 1996).

The development of wake vortex radar reflectivity models in clear air and fog in this report is dependent on output from a NASA two dimensional (2D) large eddy simulation wake vortex model referred to as the Terminal Area Simulation System (TASS) (Proctor, 1987). A vertical profile of winds and thermodynamic variables, as well as aircraft data such as weight, speed, wingspan, and initial vortex circulation are input to TASS. The wake vortex radar reflectivity models in clear air and fog use the TASS outputs to predict radar reflectivity, typically on a one-meter grid, within the wakes of the generating aircraft. TASS 2D output and consequently 2D wake vortex reflectivity models are available every 10 seconds after formation. Section 2 of this report describes the TASS outputs for clear air and fog.

In clear air, the scattering mechanism primarily results from small inhomogeneities in refractive index due to a water vapor gradient in turbulent eddies in the atmosphere. When wakes are generated in fog, liquid water that is arranged in an

ensemble of spherical drop sizes provides Rayleigh scattering. The principal radar design equation for distributed targets is the single pulse, signal-to-noise ratio equation. Assuming adequate beam and range resolution, a radar design that predicts a single pulse, signal-to-noise ratio of 1.0 (0 dB) should be capable of locating and quantifying the intensities of the wakes of aircraft.

Equations (1.1) and (1.2) are the single pulse, signal-to-noise ratio equations for clear air and fog, respectively. The second term on the right in equation (1.1) describes the performance specifications of the radar system components and the distance from the radar to the target. The last term on the right is radar volume reflectivity,  $\eta$ , which quantifies the backscattering characteristics of the target in units of  $\text{m}^{-1}$ . (Radar volume reflectivity is actually a radar cross section density in units of  $\text{m}^2 \text{m}^{-3}$ .) Radar volume reflectivity is normally referred to in the logarithmic form— $10 \log [\eta]$ —as  $\text{dB m}^{-1}$ . Section 3 of this report describes a technique for predicting  $\eta$  on a high resolution grid within the wakes of aircraft flying in clear air.

$$\frac{S}{N} = \frac{c}{256\pi^2} \bullet \frac{P_t G^2 \lambda^2 \theta^2 \frac{\tau}{2} L_s}{R^2 k T_s B} \bullet \eta \quad (\text{clear air}) \quad (1.1)$$

$$\frac{S}{N} = \frac{\pi^2 c}{1024 \ln(2)} \bullet \frac{P_t G^2 \theta^2 \tau L_s}{R^2 \lambda^2 k T_s B} \bullet |K|^2 \bullet Z \quad (\text{fog}) \quad (1.2)$$

In equation (1.2), the third term on the right is a numerical value for the dielectric properties of the fog drops;  $|K|^2$  equals approximately 0.93 for liquid water in the microwave and millimeter wave portion of the electromagnetic spectrum. The last term,  $Z$ , describes the backscattering characteristics of the ensemble of fog drops and is called the radar reflectivity factor. The units of  $Z$  are  $\text{mm}^6 \text{m}^{-3}$ . Radar reflectivity factor is also normally referred to in its logarithmic form— $10 \log [Z]$ —as  $\text{dBZ}$ . A model which predicts  $Z$  on a high resolution grid within the wakes of aircraft flying in fog is presented in Section 4 of this report.

Specification of radar wavelength, transmitter, antenna, receiver, and range for a wake vortex radar is ultimately dependent on an evaluation of the performance specification terms in equations (1.1) and (1.2). Such an evaluation is only possible when

the target characteristics ( $\eta$  or  $Z$ ) are quantified. This report focuses on the development of wake vortex models for these target terms.

## 2.0 TERMINAL AREA SIMULATION SYSTEM (TASS) MODEL OUTPUT FOR CLEAR AIR AND FOG

The TASS simulation of an aircraft wake, including both counter-rotating vortices that are contained in a descending volume of air, is generated on a 2D grid. The grid resolution typically varies between 0.75 and 2.0 meters. The TASS output provides mean thermodynamic and wind variables, as well as an estimate of the dissipation of turbulent kinetic energy; these data can be used to predict the radar reflectivity within the aircraft wake.

In the clear air case, TASS provides mean outputs of pressure (mb), temperature ( $^{\circ}\text{K}$ ), absolute humidity ( $\text{gm m}^{-3}$ ), turbulent kinetic energy (TKE) dissipation rate ( $\text{watt kg}^{-1}$ ), and horizontal and vertical winds ( $\text{m sec}^{-1}$ ) within the wake of the generating aircraft. The TASS mean outputs in fog include pressure (mb), temperature ( $^{\circ}\text{K}$ ), bulk liquid water content ( $\text{kg kg}^{-1}$ ), TKE dissipation rate ( $\text{watt kg}^{-1}$ ), and horizontal and vertical winds ( $\text{m sec}^{-1}$ ).

The wake of a C-130 observed 30 seconds after wake rollup is used throughout this report. Thirty seconds prior to the time of this example, the C-130 wake was formed at 110 meters above the surface. Thirty seconds later, the wake has descended to approximately 50 meters above the surface. The TASS grid resolution is 0.75 meters.

### 2.1 TASS Output for Clear Air

In clear air, TASS mean output includes: pressure (mb), temperature ( $^{\circ}\text{K}$ ), absolute humidity ( $\text{gm m}^{-3}$ ), turbulent kinetic energy (TKE) dissipation rate ( $\text{watt kg}^{-1}$ ), and horizontal and vertical winds ( $\text{m sec}^{-1}$ ) within the wake of the generating aircraft.

#### 2.1.1 Pressure

Figure 2–1 shows the pressure output (in millibar) for the example C-130 wake at 30 seconds after wake vortex rollup. The pressure of the ambient atmosphere decreases with height and the individual vortices are well marked by the two pressure troughs. Refractive index increases with increasing pressure. This relationship is important because small scale inhomogeneities in refractive index produce radar volume reflectivity. Therefore, the pressure gradient within the wake of the C-130 is directly

related to the reflectivity that can be observed by a radar. Note that the history of the wake descent is not obvious in Figure 2-1.

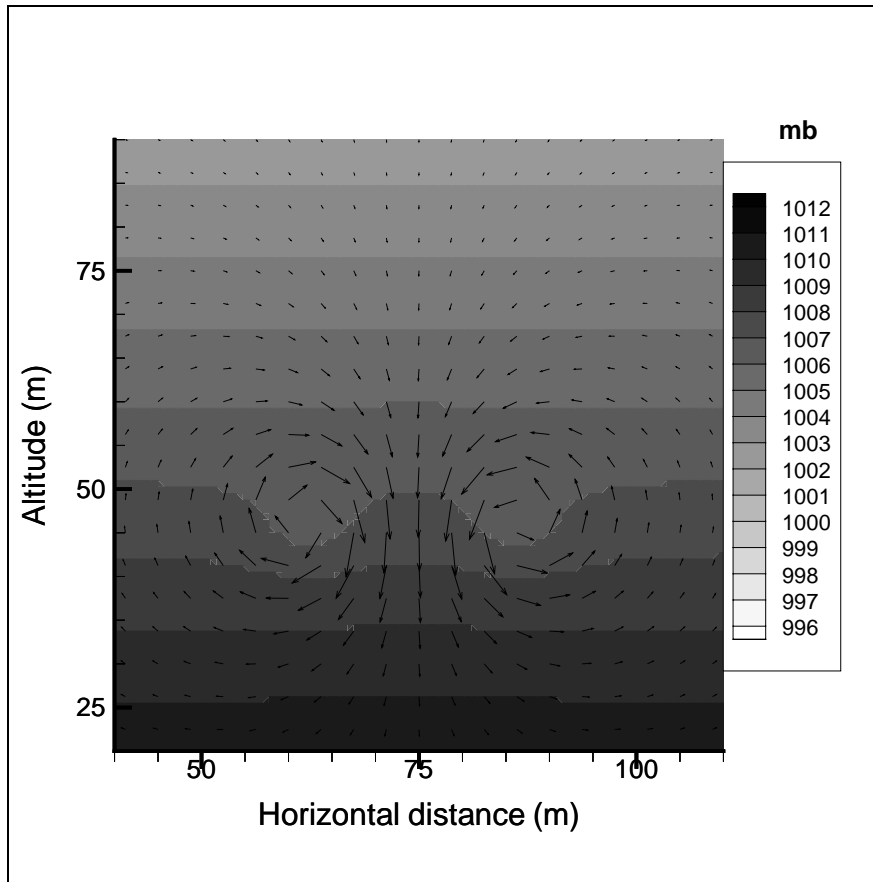


Figure 2-1. Pressure (mb) predicted by TASS in the wake of a C-130 at 30 seconds after rollup. (clear air)

### 2.1.2 Temperature

Figure 2-2 shows the TASS temperature output for the C-130 wake with the wind vectors overlaid. The left and right vortex cores are located at 62 and 86 meters, respectively, in the horizontal. Lapse rate is a term that delineates the absolute value of the vertical gradient of decreasing temperature; the lapse rate of the ambient atmosphere in which the wake is generated is  $7\text{ }^{\circ}\text{K km}^{-1}$ . Notice that the cores can be located by the small areas of  $287.8\text{ }^{\circ}\text{K}$  atmosphere. Previous anecdotal references of 5 to 10 degree temperature gradients across individual vortex cores has suggested the use of radiometry as a wake vortex sensing technique; however, this concept is not supported by the modeled temperature data displayed in Figure 2-2. Notice that the history of the wake descent is indicated in the ambient atmosphere above the wake. Refractive index, which

is directly related to the radar volume reflectivity observed by a radar, decreases with increasing temperature.

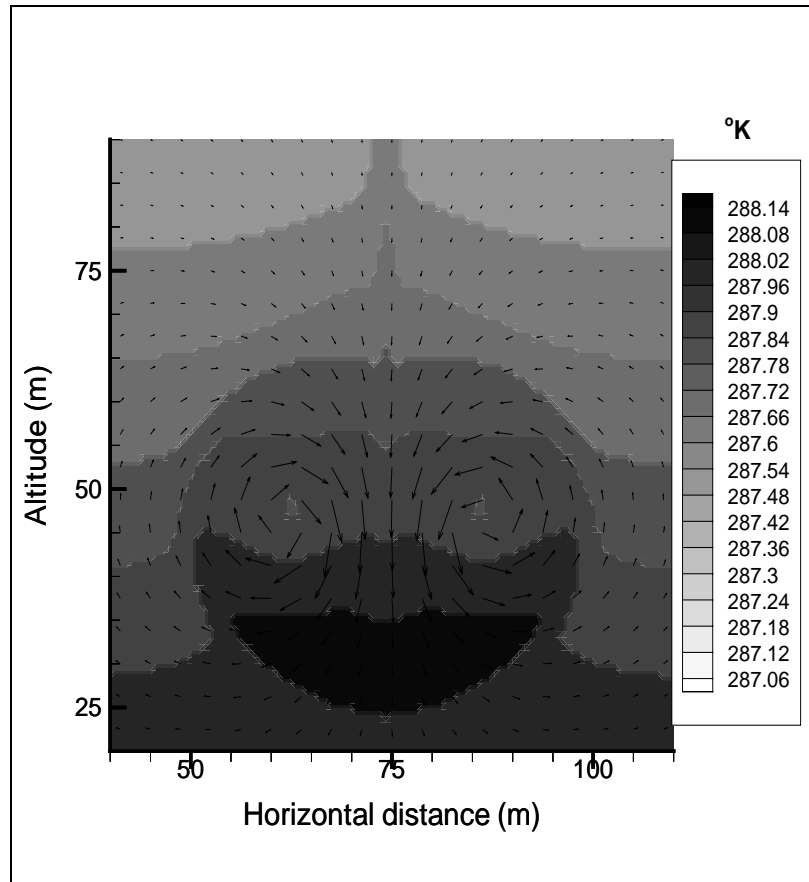


Figure 2–2. Temperature (°K) predicted by TASS in the wake of a C-130 at 30 seconds after rollup. (clear air)

### 2.1.3 Absolute Humidity

Figure 2–3 shows absolute humidity for the C-130; absolute humidity is a measure of the amount of water vapor in the atmosphere. The water vapor is conserved throughout the ambient atmosphere at approximately  $12 \text{ gm m}^{-3}$ . Figure 2–3 shows how the descending volume of air surrounding the two vortices produces a strong water vapor front that typically descends at  $1 \text{ m sec}^{-1}$  for a C-130 aircraft. Absolute humidity is highest in the lower portions of the individual vortices. The history of the wake's descent indicates inflow at the top of the descending volume of air. Refractive index, which is directly related to the radar volume reflectivity observed by a radar, increases with increasing humidity.

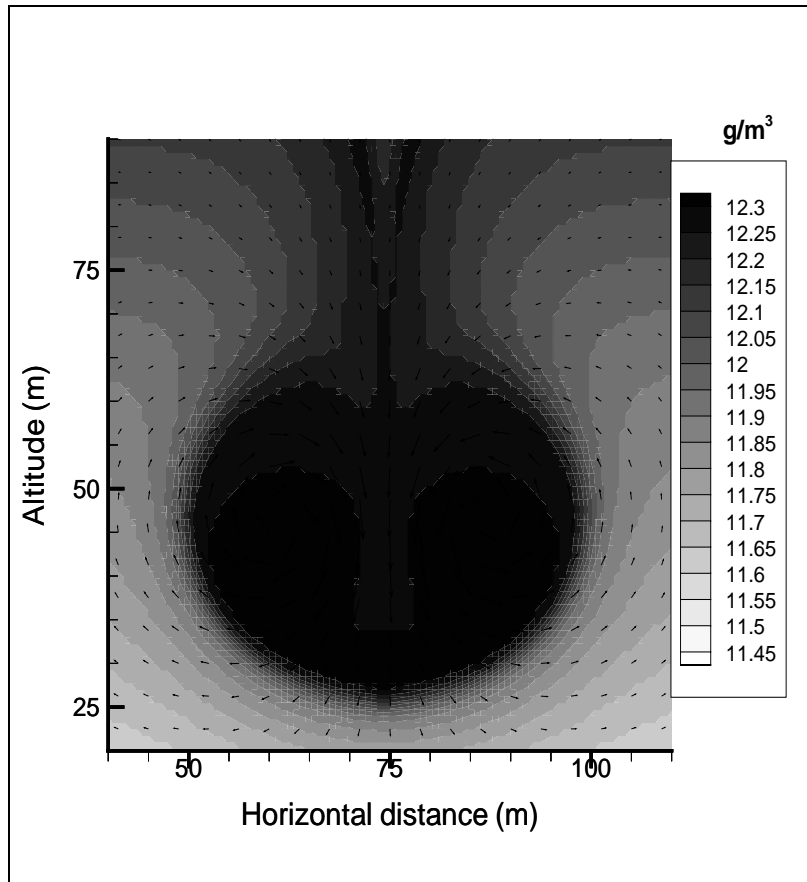


Figure 2–3. Absolute humidity ( $\text{gm m}^{-3}$ ) predicted by TASS in the wake of a C-130 at 30 seconds after rollup. (clear air)

#### 2.1.4 Turbulent Kinetic Energy (TKE) Dissipation Rate

TKE dissipation rate is a fundamental parameter in turbulence theory. In the development of a wake vortex clear air radar reflectivity model, TKE dissipation rate is used to analyze the size of the smallest scales of turbulence and to predict radar reflectivity. Smaller scales of turbulence are associated with higher values of TKE dissipation rate, and higher values of TKE dissipation rate are associated with stronger turbulence. Representative values of TKE dissipation rate are given in Table 2–1 (Trout and Panofsky, 1969).

Table 2–1. TKE dissipation rates associated with aircraft related levels of turbulence

<b>Turbulence Level</b>	<b>TKE dissipation rate (<math>\text{watt kg}^{-1}</math>)</b>
light	0.0030
moderate	0.0085
severe	0.0675

Figure 2–4 shows the TKE dissipation rate in  $\text{watts kg}^{-1}$  for the C-130 at 30 seconds after rollup. Notice that there is a band of severe turbulence around and separating the two vortices. Areas above and below the vortex cores contain TKE dissipation rates four times that found in severe turbulence.

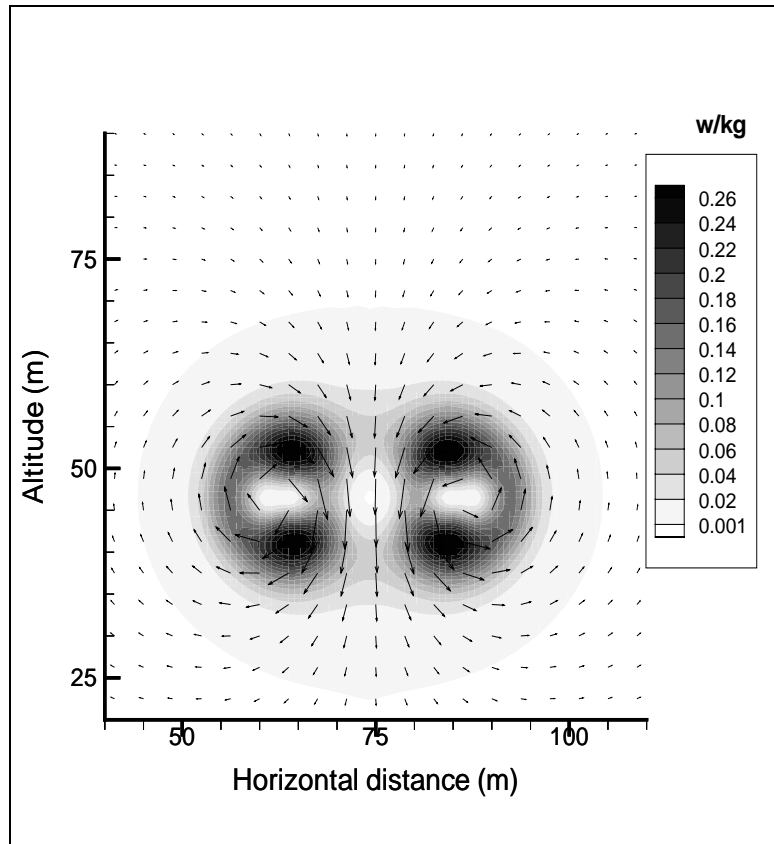


Figure 2–4. TKE dissipation rate ( $\text{watt kg}^{-1}$ ) predicted by TASS in the wake of a C-130 at 30 seconds after rollup. (clear air)

## 2.2 TASS Output for Fog

The TASS mean outputs in fog include pressure (mb), temperature ( $^{\circ}\text{K}$ ), bulk liquid water content ( $\text{kg kg}^{-1}$ ), TKE dissipation rate ( $\text{watt kg}^{-1}$ ), and horizontal and vertical winds ( $\text{m sec}^{-1}$ ). In order to produce these outputs, TASS requires vertical soundings of pressure, temperature and liquid water content,  $M$ . Figures 2–5 and 2–6 represent the vertical profiles of temperature and liquid water content in a dense advection fog that was documented at Vandenberg Air Force Base (VAFB) in August of 1992 (Zak, 1994). The data are averages at each 10 meters in the vertical over six samples that were taken approximately 10 minutes apart. The temperature inversion

shown in figure 2–5 is typical for a fog layer. In addition, liquid water content as high as  $1 \text{ gm m}^{-3}$  are observed in some advection fogs. (See figure 2–6.)

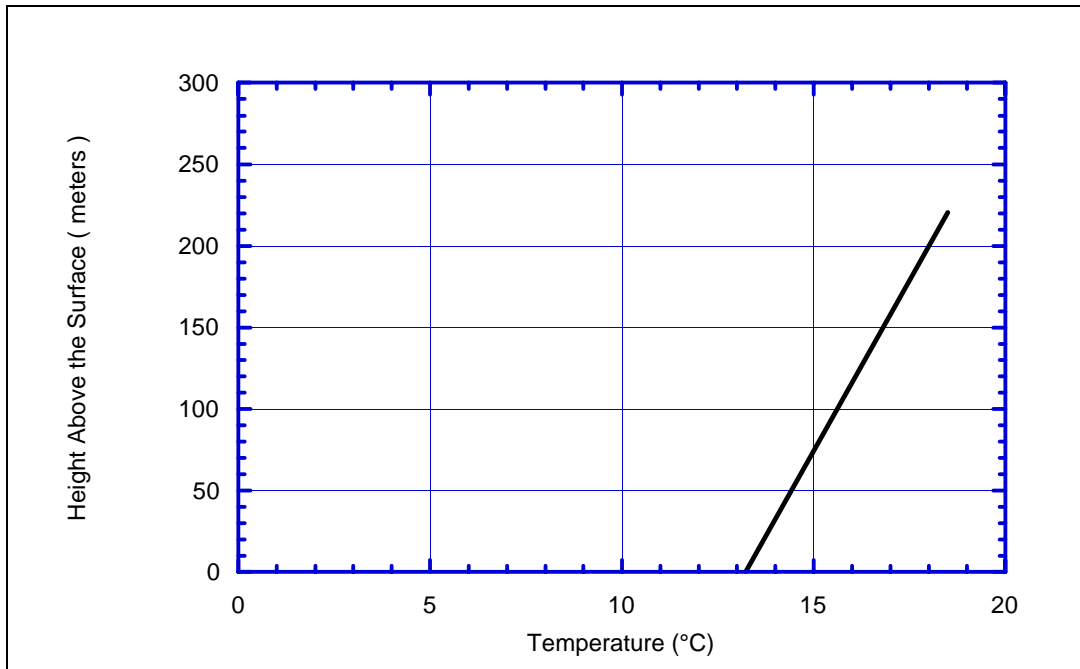


Figure 2–5. Temperature profile for the averaged VAFB fog layer.

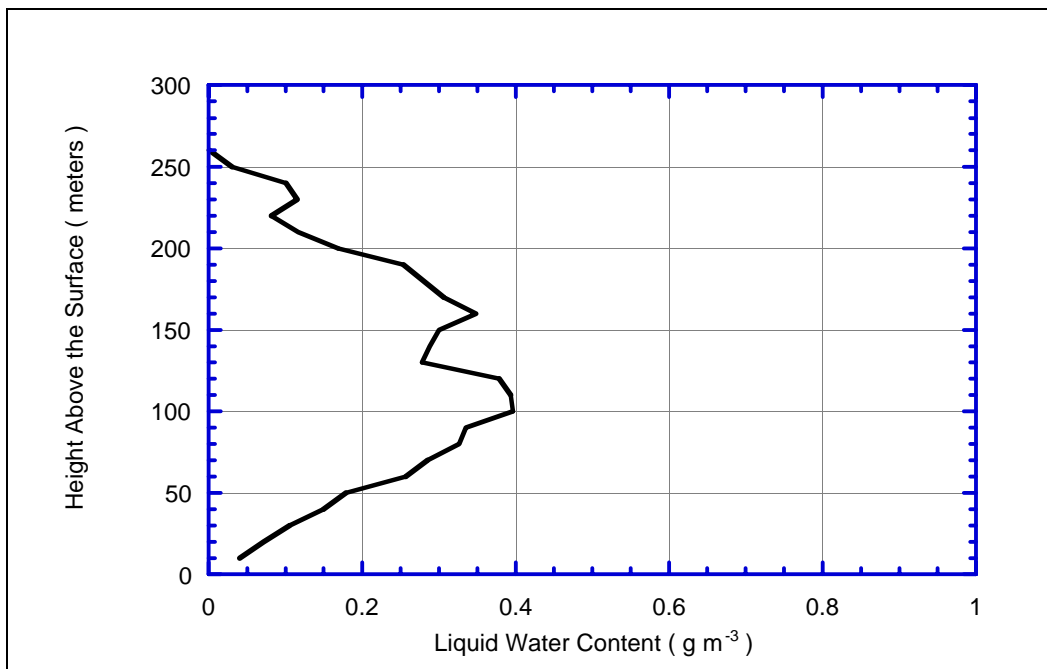


Figure 2–6. Liquid water content profile for the averaged VAFB fog layer.

Of the TASS output variables for fog conditions, only bulk liquid water content is used in deriving the reflectivity model. Figure 2–7 shows TASS output of liquid water content for the wake of a C-130 at 30 seconds after generation at the top of the fog layer described in Figures 2–5 and 2–6.

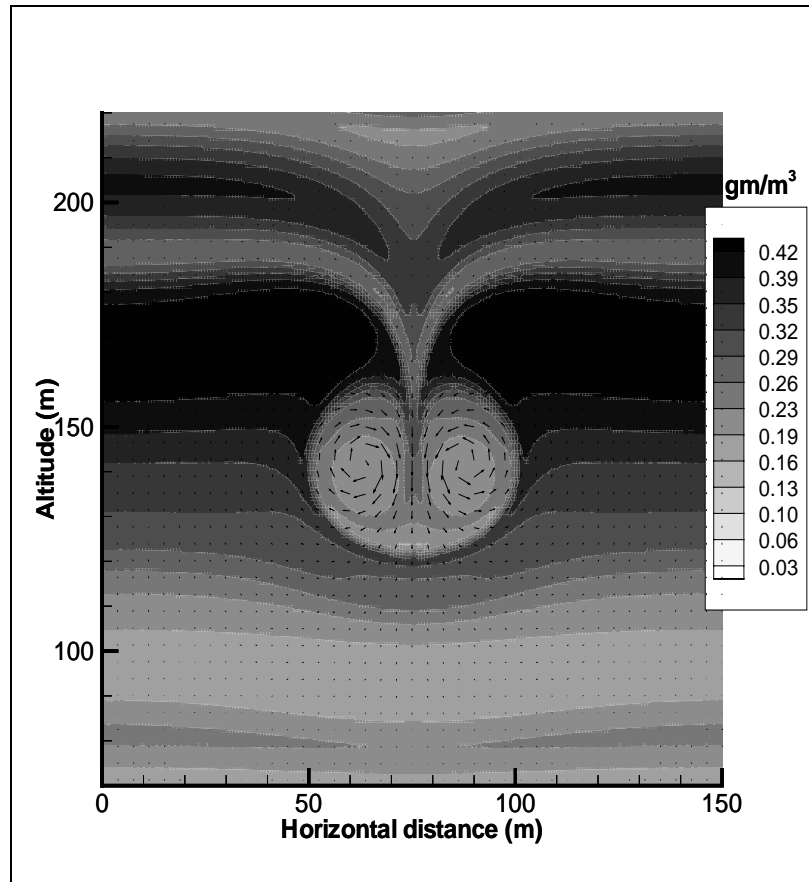


Figure 2–7. Liquid water content in the wake of a C-130 generated in the averaged VAFB fog layer. (dense advection fog)

### 2.3 TASS Wind Variables

TASS provides the horizontal (U) and vertical (W) components of the mean 2D wind field at each grid point in  $\text{m sec}^{-1}$ . Figure 2–8 depicts the mean horizontal wind speed for the C-130. Notice the areas of vertical and horizontal shear in the horizontal wind. Shear in the mean wind field is often a source of turbulence.

Figure 2–9 depicts vertical wind speed for the C-130. As with Figure 2–8, there is considerable shear in the mean vertical wind indicating potential sources of turbulence.

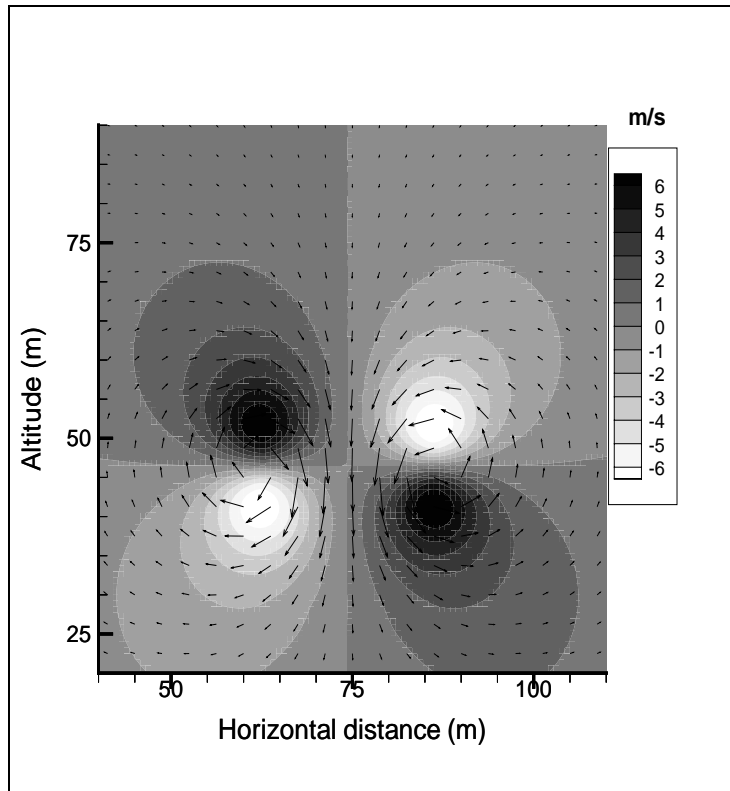


Figure 2-8. Horizontal wind speed in the wake of the C-130 at 30 sec after rollup.

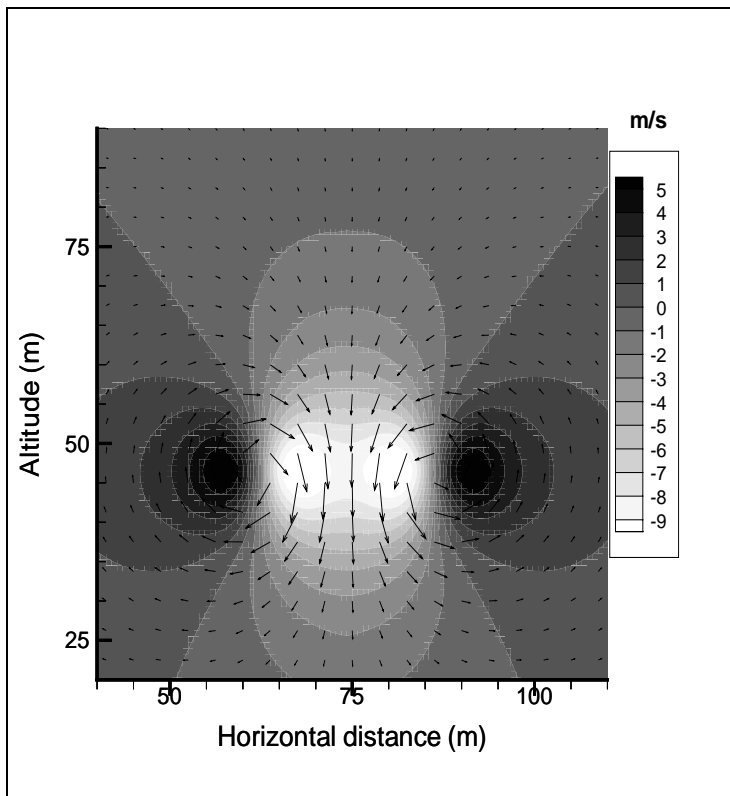


Figure 2-9. Vertical wind speed in the wake of the C-130 at 30 sec after rollup.

Figure 2–10 shows the resultant velocity vectors for the C-130. The length of the vector is proportional to the wind speed. Wind speeds as high as  $10 \text{ m sec}^{-1}$  are found on the inside edges of each vortex.

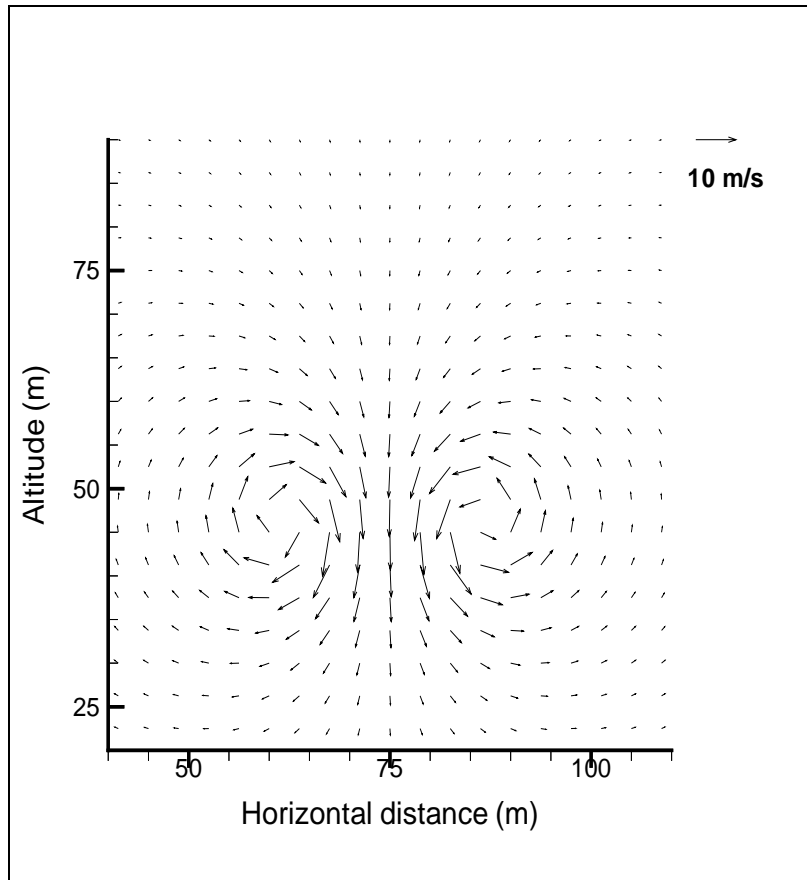


Figure 2–10. Vector plot of wind velocity in the C-130 wake at 30 sec after rollup.

In Figure 2–11, the vertical component of the wind field is plotted along a horizontal line through the vortex cores. The two “zero crossings” of vertical velocity identify the locations of the vortex cores. The adjoining maximum and minimum in vertical velocity define opposite sides of the individual vortex core walls. These maximum and minimum velocity locations indicate that the core diameters are approximately 10 meters. The data indicate a 25 meter separation between the two counter-rotating vortices. A trailing aircraft flying into the core of the left vortex would experience upward velocity on the left wing and downward velocity on the right wing resulting in an induced roll from which the aircraft may or may not be able to recover.

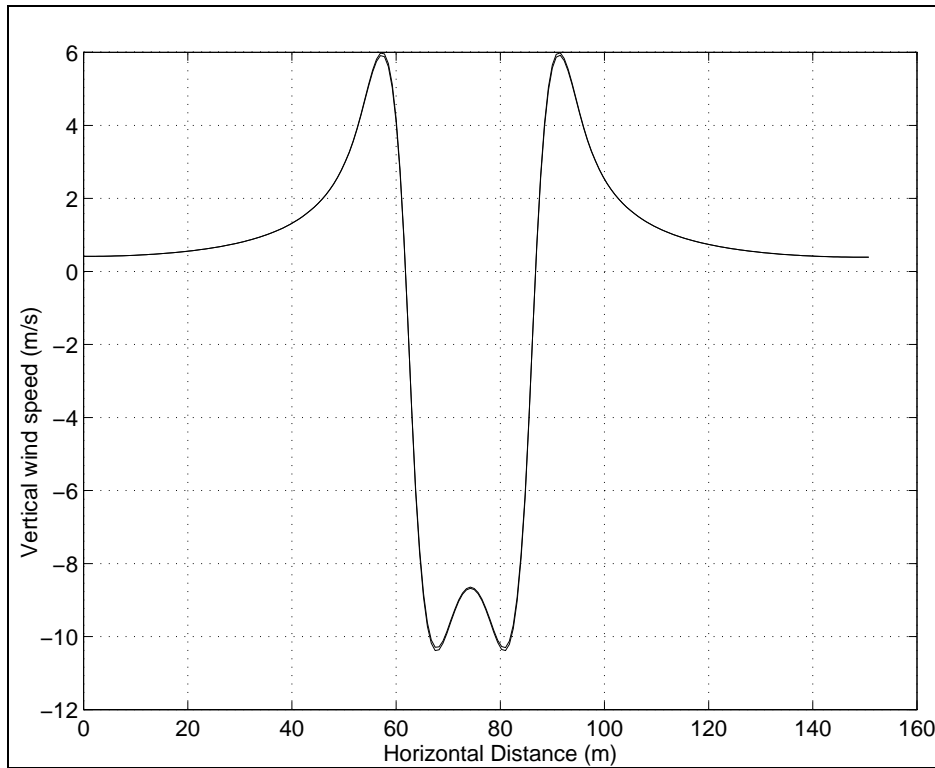


Figure 2-11. Vertical wind speed along a line through the core of the C-130 wake at 30 sec after rollup.

### 3.0 RADAR REFLECTIVITY MODEL FOR CLEAR AIR

The wake vortex radar volume reflectivity model in clear air is based on turbulence theory, in which there are always more unknowns than equations. Turbulent closure can only be accomplished with models and estimates based on intuition and experience (Tennekes and Lumley, pp. xi and 5). Closure concepts such as eddy viscosity of the atmosphere and atmospheric turbulent mixing length imitate, in a heuristic way, molecular viscosity and mean free path from the kinetic theory of ideal gases. These crude closure techniques are applied to the unique flow geometry of the wake vortex in an intuitive manner in order to infer the millimeter scale characteristics of the refractive index field from the given meter scale characteristics of mean flow and mean water vapor fields. A radar volume reflectivity model based on the turbulent production of small scale refractive index inhomogeneities must provide two products: the amplitude of  $\eta$ , and an estimate of the smallest scales of turbulence where TKE is not being dissipated through viscosity as heat.

#### 3.1 Derived Thermodynamic Variables

Potential temperature and water vapor mixing ratio can be derived from the TASS output in Section 2.1 for clear air. These derived thermodynamic variables—on the same grid structure as the TASS output—are useful in the development of the radar reflectivity model for clear air.

##### 3.1.1 Potential Temperature

The potential temperature,  $\theta$ , of a parcel of air is defined as the temperature that the parcel of air would have if it were expanded or compressed adiabatically from its existing pressure and temperature to a standard pressure of 1000 mb (Wallace and Hobbs, 1977). In an adiabatic or neutral atmosphere, the temperature lapse rate is  $9.8 \text{ }^\circ\text{K km}^{-1}$  and potential temperature is conserved. Potential temperature can be calculated from the expression in equation (3.1).

$$\theta = T \left( \frac{p_0}{p} \right)^{R_d/c_p} \quad (3.1)$$

where  $T \equiv$  temperature ( $^{\circ}\text{K}$ );  $p_0 \equiv$  reference pressure = 1000 mb;  $p \equiv$  pressure (mb);  $R_d \equiv$  dry air gas constant =  $287 \text{ J deg}^{-1} \text{ kg}^{-1}$ ; and  $c_p \equiv$  specific heat at constant pressure =  $1004 \text{ J deg}^{-1} \text{ kg}^{-1}$ .

Figure 3–1 shows the potential temperature of the C-130 wake calculated from equation (3.1). The slight increase in potential temperature with height of the ambient atmosphere indicates that the layer is near neutral. Notice that there are areas of buoyancy in the wake indicated by negative vertical gradients of potential temperature. The stratification effects result from the stratification of temperature and pressure in the wake (see figures 2–1 and 2–2).

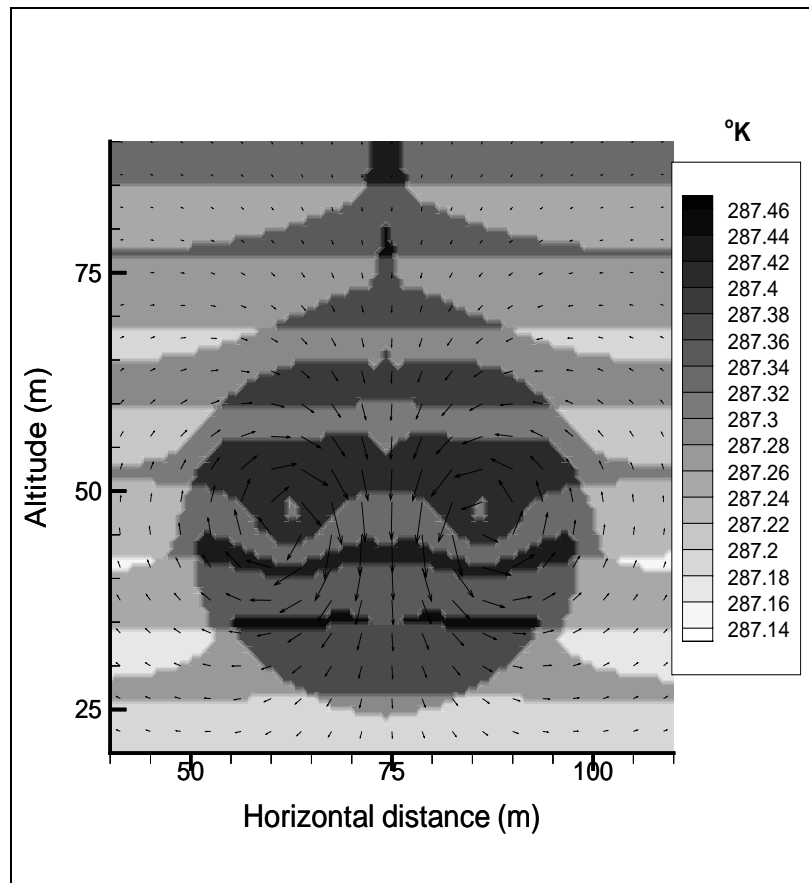


Figure 3–1. Potential temperature ( $^{\circ}\text{K}$ ) in the wake of a C-130 at 30 seconds after rollup.

### 3.1.2 Water Vapor Mixing Ratio

Water vapor mixing ratio ( $w$  in  $\text{kg kg}^{-1}$ ) is the ratio of the mass of water vapor to the mass of the dry air containing the water vapor (Hess, 1979) as given in equation (3.2). Typical atmospheric values vary between 1 and  $30 \text{ gm kg}^{-1}$ .

$$w = \frac{\rho_v}{\rho_d} \quad (3.2)$$

where  $\rho_v \equiv$  absolute humidity ( $\text{kg m}^{-3}$ ); and  $\rho_d \equiv$  density of dry air ( $\text{kg m}^{-3}$ ).

The density of dry air may be calculated from temperature, pressure, and the ideal gas law (Wallace and Hobbs, 1977) as given in equation (3.3). Figure 3–2 shows the dry air density for the C-130 wake.

$$\rho_d = \frac{p}{R_d T} \quad (3.3)$$

where  $p \equiv$  pressure (Pa);  $R_d \equiv$  dry air gas constant =  $287 \text{ J deg}^{-1} \text{ kg}^{-1}$ ; and  $T \equiv$  temperature ( $^{\circ} \text{K}$ ).

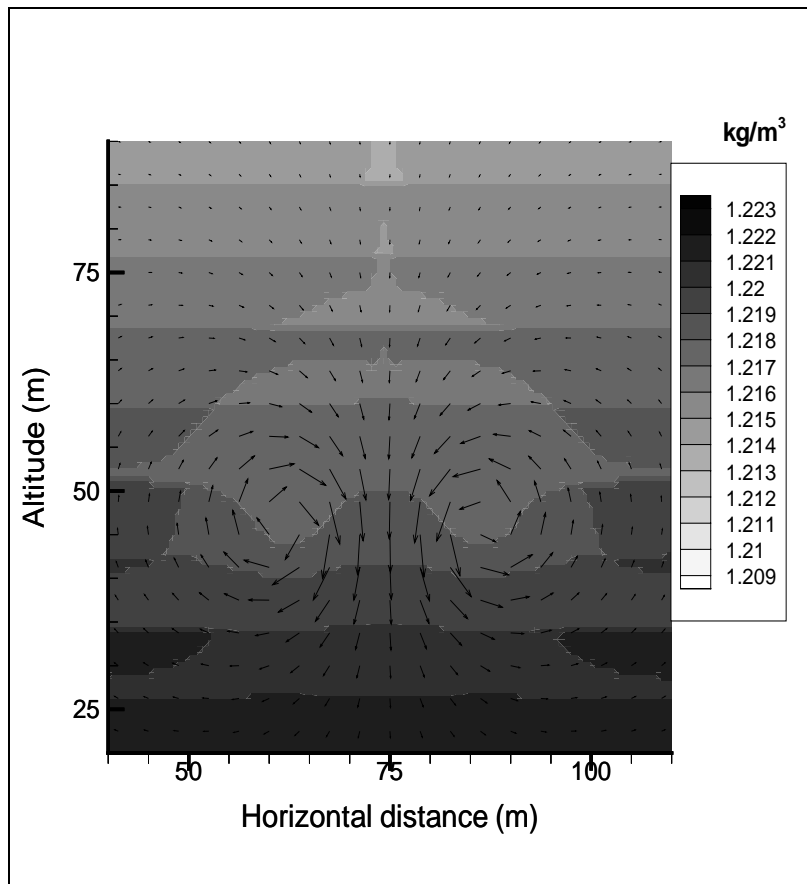


Figure 3–2. Dry air density ( $\text{kg m}^{-3}$ ) in the wake of a C-130 at 30 seconds after rollup.

Water vapor mixing ratio is then given by equation (3.4).

$$w = \frac{R_d T \rho_v}{p} \quad (3.4)$$

In the near neutral ambient atmosphere, vertical gradients of water vapor mixing ratio are very small. In Figure 3–3, notice how the descending volume of air associated with the wake has created large gradients in the mean water vapor mixing ratio field. These gradients in the humidity field translate into significant gradients in refractive index. The radar volume reflectivity along this humidity front is higher than that immediately outside the wake vortex core wall.

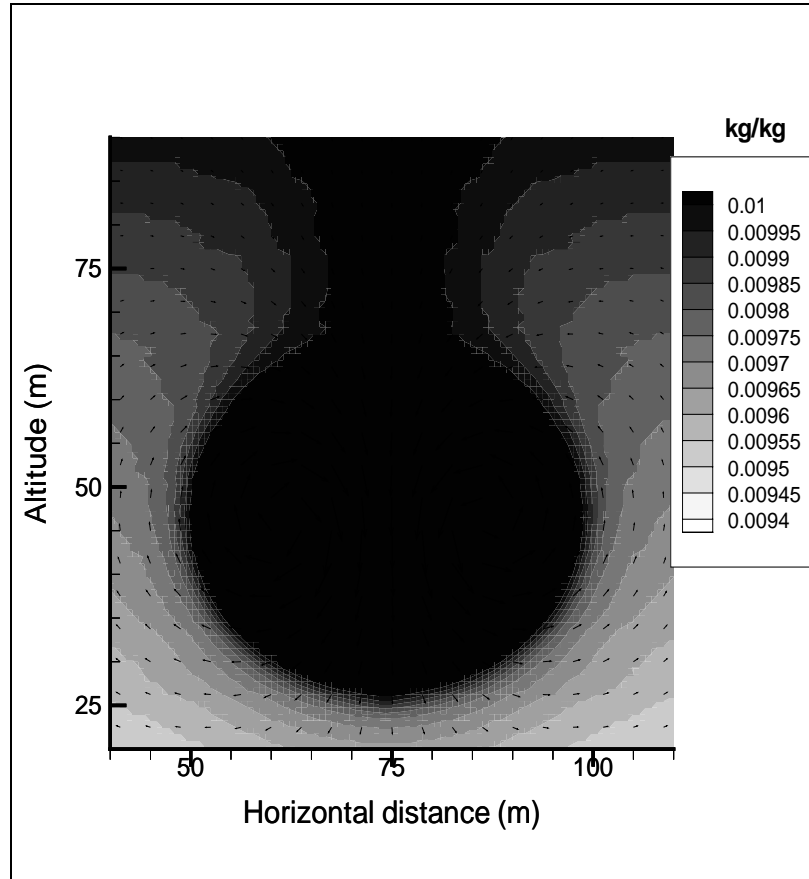


Figure 3–3. Water vapor mixing ratio ( $\text{kg kg}^{-1}$ ) in the wake of a C-130 at 30 seconds after rollup.

### 3.2 Refractive Index of the Clear Atmosphere

The refractivity,  $N$ , of the clear atmosphere is a function of atmospheric pressure, temperature, and an appropriate humidity variable, such as partial pressure due to water vapor,  $e$  (Doviak and Zrnic, 1984). Refractivity can be calculated from equation (3.5).

$$N = \left( \frac{77.6}{T} \right) \left( p + \frac{4810e}{T} \right) \quad (3.5)$$

where  $N \equiv (n-1) \times 10^6$ ;  $n \equiv$  refractive index of the atmosphere  $= (\epsilon_r)^{1/2}$ ;  $\epsilon_r \equiv$  relative permittivity of the atmosphere;  $T \equiv$  Temperature ( $^{\circ}\text{K}$ );  $p \equiv$  pressure (mb); and  $e \equiv$  partial pressure due to water vapor (mb).

The partial pressure due to water vapor is related to water vapor mixing ratio and total pressure by equation (3.6) (Wallace and Hobbs, 1977).

$$e = \frac{w}{w + 0.622} p \quad (3.6)$$

where  $w \equiv$  water vapor mixing ratio ( $\text{kg kg}^{-1}$ ); and  $p \equiv$  pressure (mb).

Equations (3.5) and (3.6) can be combined to describe refractivity in terms of atmospheric temperature, pressure, and water vapor mixing ratio. Figure 3–4 shows the refractivity calculated from equation (3.7) for the C-130.

$$N = \frac{77.6p}{T} \left( 1.0 + \frac{4810w}{T[w + 0.622]} \right) \quad (3.7)$$

where  $T \equiv$  Temperature ( $^{\circ}\text{K}$ );  $p \equiv$  pressure (mb); and  $w \equiv$  water vapor mixing ratio ( $\text{kg kg}^{-1}$ ).

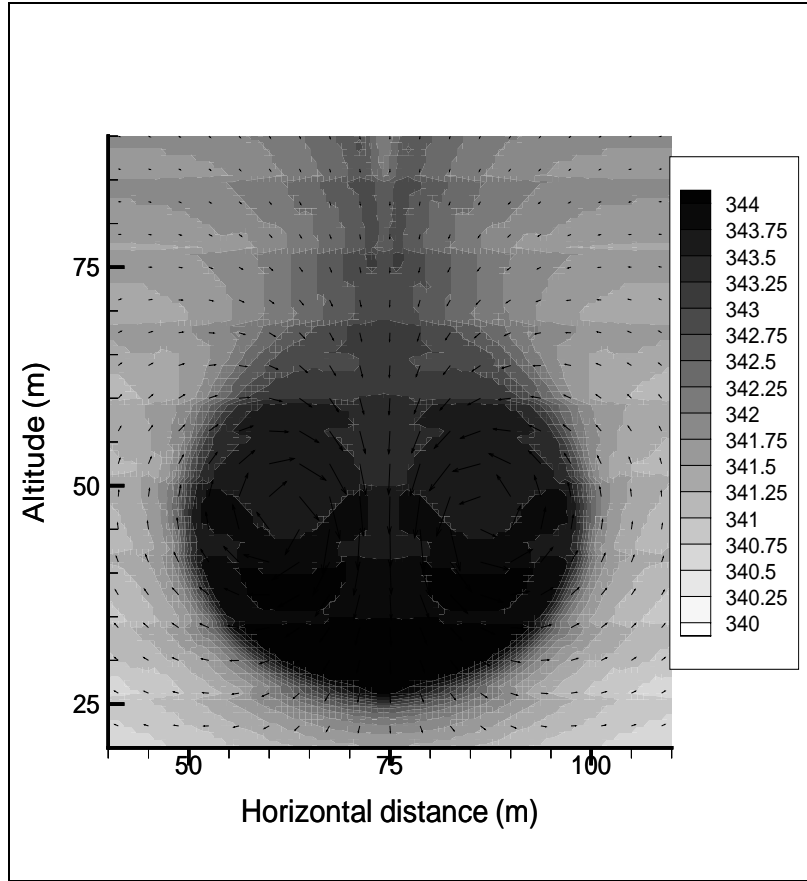


Figure 3–4. Refractivity in the wake of a C-130 at 30 sec after rollout.

As parcels of air are displaced vertically in the atmosphere, the pressure within the parcel is continually equalized with the surrounding air. This results in changes in the temperature and water vapor pressure of the parcel of air. Since a property is considered to be conserved if it's characteristics do not change when the parcel of air is moved within the atmosphere, temperature, water vapor pressure and, hence, refractivity are not conserved properties. The necessity for a conserved property led to the definition of potential refractive index,  $\Phi$ , as given in equation (3.8).

$$\Phi = 1 + 10^{-6} \left( \frac{77.6}{\theta} \right) \left( p_0 + \frac{4810e_0}{\theta} \right) \quad (3.8)$$

where  $\theta = T(p_0 / p)^{0.286} \equiv$  potential temperature at the reference pressure,  $p_0$ ;  $p_0 = 1000$  mb; and  $e_0 \equiv$  potential water vapor pressure (mb) at the reference pressure,  $p_0$ . Potential refractive index is a conserved property because  $\theta$  and  $p_0$  are conserved properties of the parcel of air (Doviak and Zrnic, 1984).

Potential water vapor pressure can be obtained from equation (3.9).

$$e_0 \equiv e \left( \frac{1000}{p} \right) \quad (3.9)$$

where  $e \equiv$  water vapor pressure (mb).

Equations (3.6), (3.8), and (3.9) can be combined to form equation (3.10), which describes potential refractive index in terms of potential temperature and water vapor mixing ratio. Figure 3–5 shows the potential refractive index in the wake of the C-130, as calculated from equation (3.10).

$$\Phi = 1 + 10^{-6} \left\{ \frac{77.6 \times 10^3}{\theta} \left( 1 + \frac{4810w}{\theta[w + 0.622]} \right) \right\} \quad (3.10)$$

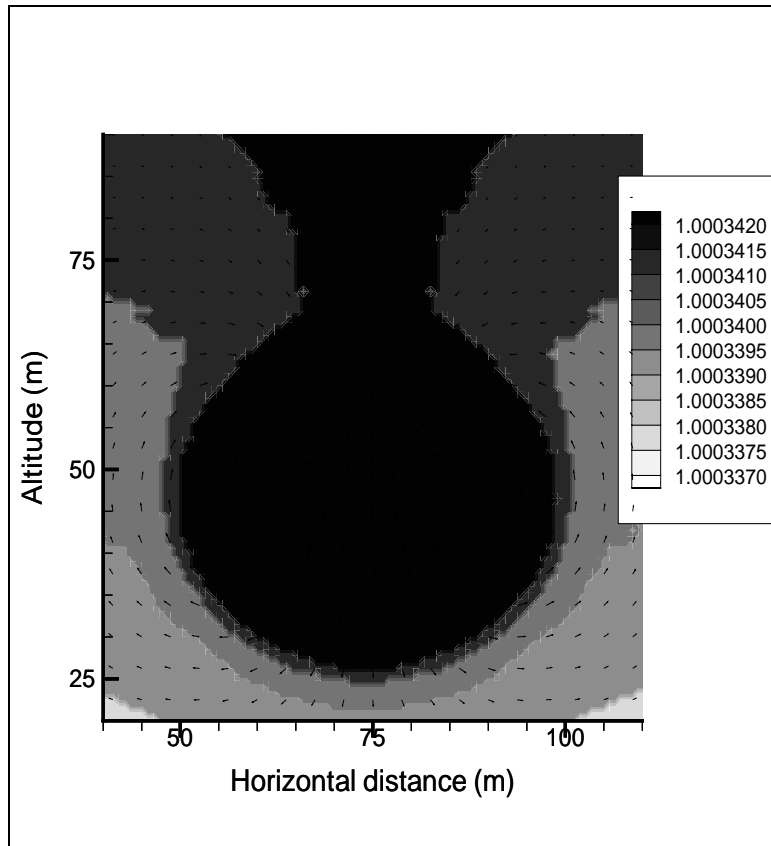


Figure 3–5. Potential refractive index in the wake of a C-130 at 30 sec after rollup.

### 3.3 Scales of Turbulence in the Clear Atmosphere

Prediction of radar volume reflectivity in clear air assumes that the primary contributors to backscattering are turbulent eddies that are one-half the radar wavelength

in diameter. These turbulent eddies produce small scale discontinuities of refractive index, which contribute to the radar volume reflectivity. A continuum of turbulent eddy sizes are continually being produced and destroyed by the turbulence. Figure 3–7 is a simplistic representation of such a turbulent wind eddy.

The eddy in figure 3–7 contains an atmosphere with a refractive index different than the surroundings. As shown in the previous section, atmospheric refractive index is a function of temperature, pressure, and water vapor mixing ratio. Therefore, an electromagnetic wave incident on the eddy from the left will experience partial reflection. The portion of the energy that continues through the eddy will experience a similar reflection upon exiting and will experience a 360 degree phase shift from the point of initial reflection.

Turbulent kinetic energy (TKE) is dissipated by the smallest eddies through viscosity as heat. If half-radar wavelength eddies are dissipating TKE, then the radar wavelength will be too small to detect the turbulence. Therefore, a scales of turbulence analysis technique was developed to determine the maximum radar frequency that could be used for the detection of wake vortices in clear air.

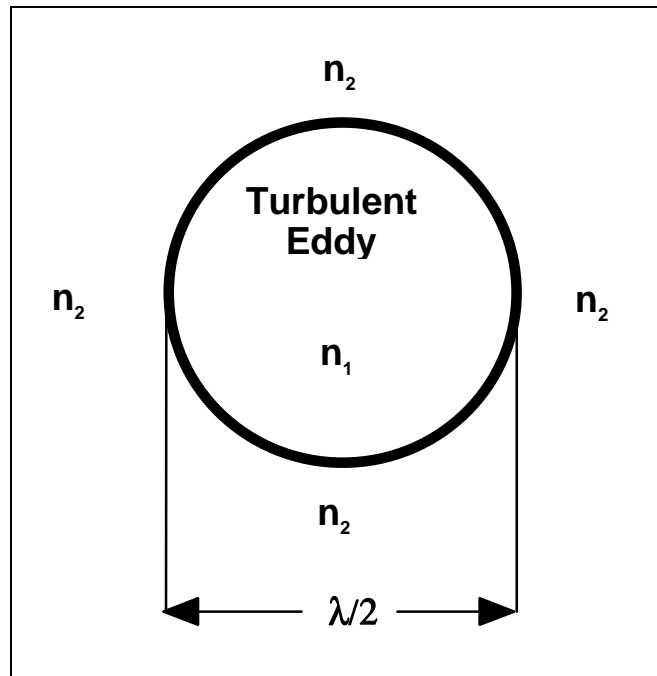


Figure 3–7. Schematic representation of a turbulent eddy that is one-half the radar wavelength in diameter. ( $n_1 \equiv$  refractive index inside the eddy;  $n_2 \equiv$  refractive index surrounding the eddy)

In 1926, Richardson hypothesized that the larger scale turbulent eddies break down into smaller and smaller eddies in a “cascading” effect until the TKE of the flow is viscously dissipated as heat at very small eddy sizes (Sorbjan, 1989). In 1941, Kolmogorov introduced the inertial subrange hypothesis that predicted the existence of an inertial subrange of turbulent eddy sizes, in which the energy is transferred from eddy to smaller eddy without dissipation in large Reynolds number flows (Sorbjan, 1989).

Figure 3–8 represents the distribution of TKE by eddy diameter ( $d$ ). The Integral scale, or outer scale as it is referred to in Russian literature, represents the largest turbulent eddy size in the flow. For the entire wake of an aircraft, this size eddy would be on the order of a wingspan. For individual vortices, the integral scale is related to the vortex core diameter. The inertial subrange extends from the integral scale to the Taylor microscale.

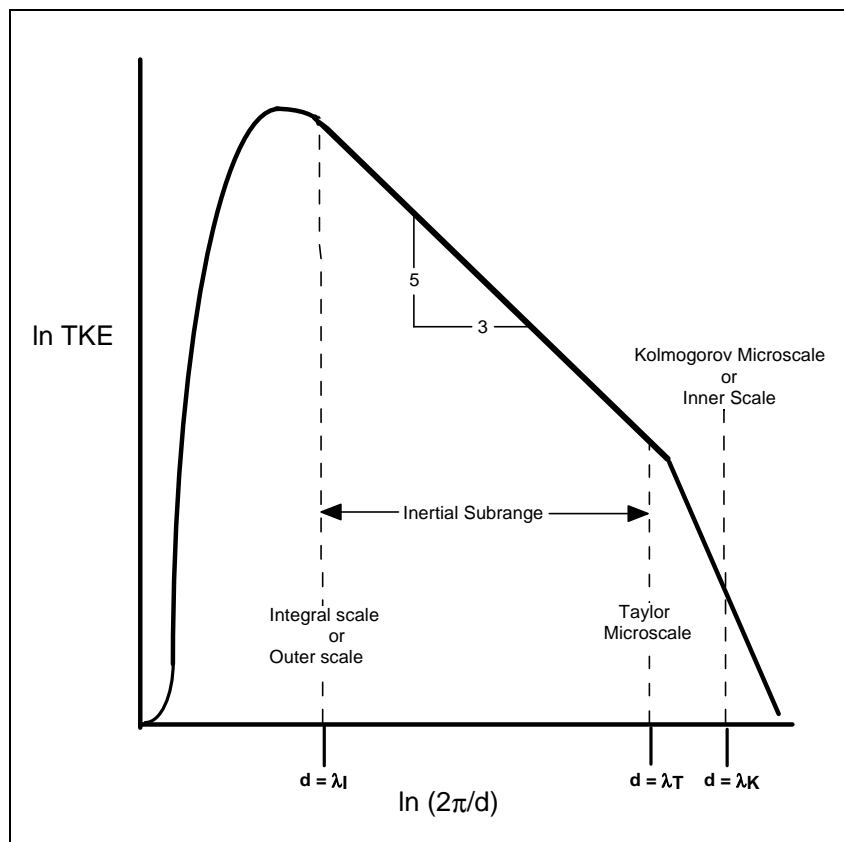


Figure 3–8. Turbulent Kinetic Energy Spectrum as a function of turbulent eddy wavenumber. ( $d = \lambda/2$ )

The volume reflectivity model for clear air assumes that turbulent eddies with diameters equal to one-half the radar wavelength are in the inertial subrange of turbulence. Radar wavelengths that are smaller than twice the Taylor microscale will not meet this modeling assumption. As radar wavelengths decrease past twice the Taylor microscale towards twice the Kolmogorov microscale, viscous dissipation dominates the turbulence and reduces the production of refractive index inhomogeneities responsible for radar volume reflectivity. The reduction in volume reflectivity at higher radar frequencies translates into a need for radars with impractical transmitter power-antenna gain products (Cohn, 1991, 1994). Detection of half-radar wavelength diameter turbulent wind eddies that are the same size as or smaller than the Kolmogorov microscale requires a prohibitively expensive radar with a large antenna and a megawatt-level transmitter.

The Taylor microscale represents the smallest turbulent eddy size where viscous effects are not important and where TKE is not being dissipated. The Taylor microscale is then one-half the shortest wavelength of a practical radar that could be used to detect the wake. The Kolmogorov microscale, referred to as the inner scale in Russian literature, is calculable from TASS output at each TASS gridpoint. Thus, the Taylor microscale can be estimated by calculating the Kolmogorov microscale.

The Kolmogorov microscale ( $\lambda_K$ ) can be calculated from equation (3.11) and defines the turbulent wind eddy dimension below which viscous dissipation as heat begins to annihilate the turbulence (Pasquill and Smith, 1983).

$$\lambda_K = \left( \frac{v^3}{\varepsilon} \right)^{1/4} \quad (\text{meter}) \quad (3.11)$$

where  $\varepsilon \equiv$  TKE dissipation rate (watt kg<sup>-1</sup>); and  $\nu \equiv$  kinematic viscosity of the atmosphere (m<sup>2</sup> sec<sup>-1</sup>).

Kinematic viscosity,  $\nu$ , is equal to 10<sup>-5</sup> at 288 °K and 1013.25 mb. It may be calculated at any other temperature and pressure by using equation (3.12).

$$\nu = 10^{-5} \left( \frac{T}{288} \right)^{3/2} \left( \frac{1013.25}{p} \right) \quad (3.12)$$

Figure 3–9 displays the kinematic viscosity field for the C-130. The resulting Kolmogorov microscale is calculated from equation (3.11) and shown in figure 3–10.

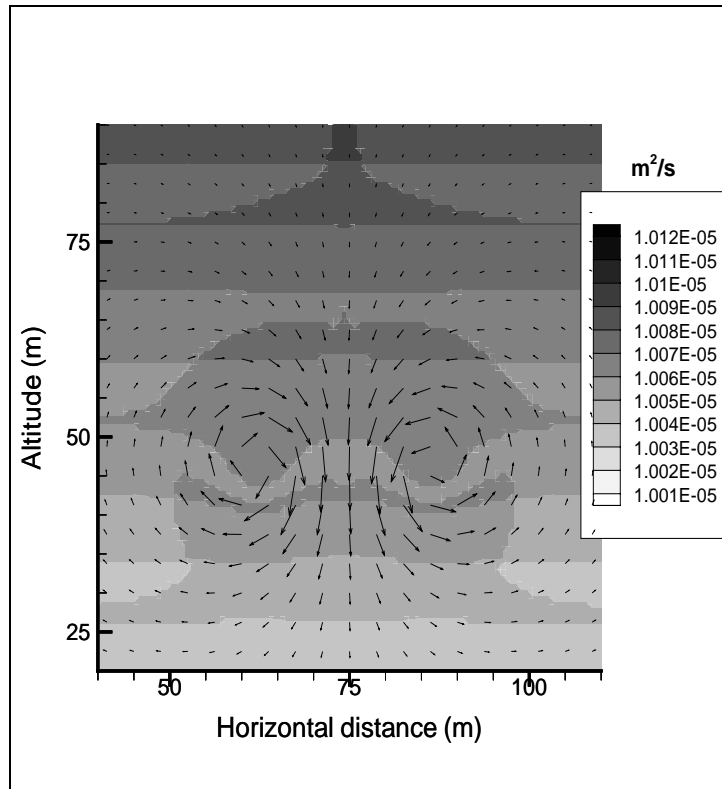


Figure 3-9. Kinematic viscosity in the wake of a C-130 at 30 seconds after rollup.

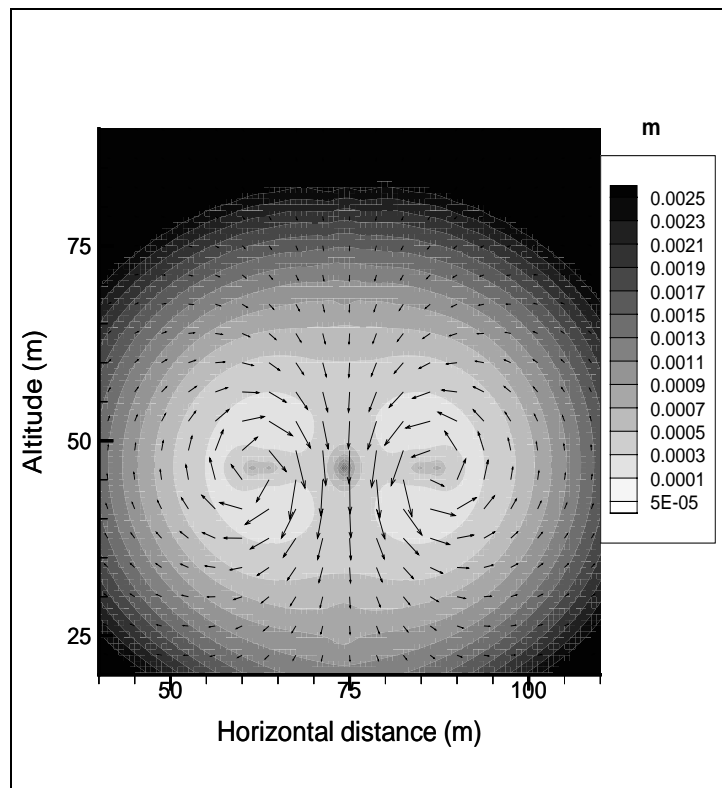


Figure 3-10. Kolmogorov microscale in the wake of a C-130 at 30 seconds after rollup.

Recall that the Taylor microscale is one-half the shortest wavelength that could be used to detect the wake using a practical radar. In order to describe an upper radar frequency for detection of clear air turbulence in the free atmosphere,  $5\pi$  has been used as the ratio of the Taylor microscale to the Kolmogorov microscale (Doviak and Zrnic, 1984). This leads to an equation for the maximum radar frequency given in equation (3.13), which is evaluated for the C-130 in Figure 3–11.

$$f_{\max} = \frac{c}{2d}$$

$$f_{\max} = \frac{c}{2\lambda_T} \tag{3.13}$$

$$f_{\max} = \frac{c}{10\pi\lambda_K}$$

where  $c \equiv$  speed of light =  $3.0 \times 10^8$  m sec<sup>-1</sup>;  $d \equiv$  diameter of turbulent eddy;  $\lambda_T \equiv$  Taylor microscale; and  $\lambda_K \equiv$  Kolmogorov microscale.

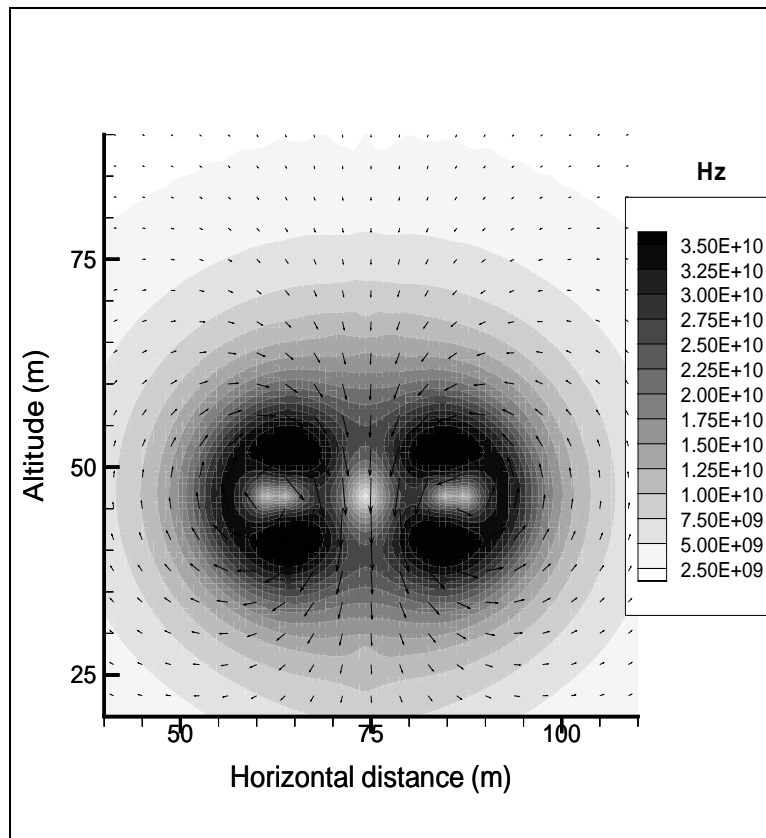


Figure 3–11. The maximum radar frequency based on  $5\pi$  times the Kolmogorov microscale in the C-130 wake.

The  $5\pi$  ratio between the Taylor and Kolmogorov microscales used in equation (3.13) is based on a convective model (Hill, 1978). However, figure 2–4 gives no indication of strong, buoyancy-driven turbulence; and, hence, the ratio  $5\pi$  may not be appropriate for the wind shear production of turbulence in an aircraft wake.

The ratio of the Taylor microscale to the Kolmogorov microscale in locally isotropic turbulence is given by equation (3.14) (Tennekes and Lumley, 1987).

$$\frac{\lambda_T}{\lambda_K} = \left( \frac{ul}{\nu} \right)^{1/4} \quad (3.14)$$

where  $u \equiv$  turbulent velocity scale;  $l \equiv$  turbulent mixing length; and  $\nu \equiv$  kinematic viscosity.

The turbulent mixing length is the average distance an eddy travels before giving up its momentum to the surroundings (Brown, 1991). For the C-130, the average distance from the core wall to a point where the momentum is reduced by  $e^{-1}$  is 3.5 meters. In equation (3.15), the turbulent velocity scale,  $u$ , is approximated by the product of the turbulent mixing length and the average shear in the mean wind field at the core wall (Sorbjan, 1989).

$$u \approx l \frac{du}{dz} \quad (3.15)$$

For the C-130 wake,  $u$  is equal to  $3.9 \text{ m sec}^{-1}$ . Assuming that the minimum radar half wavelength is equal to the Taylor microscale in equation (3.14), equation (3.16) predicts the maximum radar frequency based on the turbulent velocity and mixing length. Figure 3–12 shows an evaluation of equation (3.16) for  $l = 3.5 \text{ m}$  and  $u = 3.9 \text{ m sec}^{-1}$ .

$$f_{\max} = \frac{c}{2 \left( \frac{ul}{\nu} \right)^{1/4} \lambda_K} \quad (3.16)$$

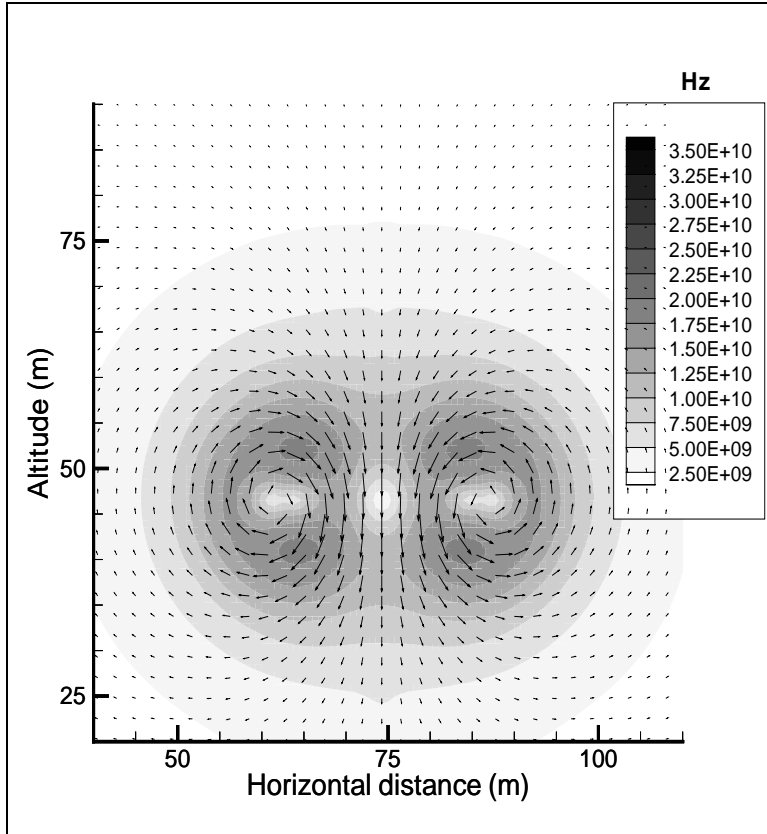


Figure 3–12. The maximum radar frequency based on the turbulent velocity and mixing length in the C-130 wake. ( $u = 3.9 \text{ m sec}^{-1}$ ;  $l = 3.5 \text{ m}$ )

### 3.4 Volume Reflectivity in the Clear Atmosphere

The following development of the first clear air radar reflectivity model for the wakes of aircraft is dependent on the assumption that the reflectivity is due to the turbulent production of refractive index discontinuities with spatial dimensions near one-half the radar wavelength. It is further assumed that these one-half radar wavelength turbulent wind eddies are in the inertial subrange of the turbulent eddy wave number spectrum. With these assumptions, we can use equation (3.17), which relates volume radar reflectivity to refractive index structure constant and radar wavelength (Tatarski, 1959).

$$\eta = 0.38C_n^2 \lambda^{-1/3} \quad (\text{m}^{-1}) \quad (3.17)$$

where  $C_n^2 \equiv$  refractive index structure constant ( $\text{m}^{-2/3}$ ); and  $\lambda \equiv$  radar wavelength (meter).

As radar frequency increases and half radar wavelength turbulent eddies move from the Taylor microscale to the Kolmogorov microscale, equation (3.17) overestimates

radar volume reflectivity. Radar volume reflectivity for distributed targets is a radar cross section density in  $\text{m}^2 \text{m}^{-3}$ . The corresponding radar sample volume is bounded by the antenna beam dimensions and the radar range resolution.

Refractive index structure constant is a wavelength-independent measure of the strength of the refractive index fluctuations;  $C_n^2$  has units of  $\text{m}^{-2/3}$ . The development strategy for the radar reflectivity model is to evaluate the refractive index structure constant from the thermodynamic and wind fields derived from TASS output at each grid point, and then to evaluate equation (3.17) at each grid point. The scales of turbulence analysis and subsequent maximum radar frequency prediction at each grid point must be considered when equation (3.17) is calculated at each grid point.

A relationship for refractive index structure constant is given in equation (3.18) (Tatarski, 1961).

$$C_n^2 = a^2 \epsilon_N \epsilon^{-2/3} \quad (3.18)$$

where  $a^2 = \text{constant} \approx 3.6$ ;  $\epsilon \equiv \text{TKE eddy dissipation rate (watt kg}^{-1}\text{)}$ ; and  $\epsilon_N \equiv \text{rate of reduction of inhomogeneity in the refractive index field}$ .

The Reynolds convention (Nieuwstadt and van Dop, 1982) is used to describe the instantaneous variables in terms of a mean plus a fluctuating or turbulent component:

$$\phi = \Phi + \phi \text{ (potential refractive index)}$$

The uppercase, or average, components are the TASS output variables. The lower case, or turbulent, components produce the small scale refractive index discontinuities that provide the clear air scattering mechanism. This model relates the fluctuating, or turbulent, component to the mean value available from TASS by a first-order turbulence closure technique called eddy diffusivity closure.

Potential refractive index, derived from the TASS output, can be used with the equation for the local rate of change of the variance of potential refractive index (Tennekes and Lumley, 1987) to obtain  $\epsilon_N$ , the rate of reduction of inhomogeneity in the refractive index field;  $\epsilon_N$  is required to evaluate equation (3.18) (Ottersten, 1969).

$$\frac{1}{2} \frac{\partial \overline{\phi^2}}{\partial t} = -\frac{1}{2} U_i \frac{\partial \overline{\phi^2}}{\partial x_i} - \overline{u_i \phi} \frac{\partial \Phi}{\partial x_i} - \frac{1}{2} \frac{\partial \overline{u_i \phi^2}}{\partial x_i} - \epsilon_N \quad (3.19)$$

where  $\phi \equiv$  instantaneous potential refractive index;  $\Phi \equiv$  mean potential refractive index;  $U \equiv$  mean horizontal component of the wind;  $u \equiv$  instantaneous horizontal component of the wind; and  $\varepsilon_N \equiv$  rate of reduction of inhomogeneity in the refractive index field.

The first term on the right side of equation (3.19) is an advection term that includes the average wind and the turbulent component of potential refractive index. The second term is a production term that contains the average potential refractive index and the covariance of the fluctuating components of wind and potential refractive index, and the third term is a turbulent transport term containing all turbulent components. Assuming steady state, two dimensional flow and that production equals dissipation reduces equation (3.19) to equation (3.20).

$$\varepsilon_N = -\overline{u\phi} \frac{\partial\Phi}{\partial x} - \overline{w\phi} \frac{\partial\Phi}{\partial z} \quad (3.20)$$

where  $w$  is the instantaneous vertical component of the wind.

The covariances in equation (3.20) can be related to the mean variables scalar eddy diffusivity closure (Nieuwstadt and van Dop, 1982). This technique was first used by Boussinesq in 1877 (Brown, 1991) to relate eddy stress to the mean wind shear and an exchange coefficient,  $K_\phi$ , as in equations (3.21) and (3.22).

$$\overline{u\phi} = -K_\phi \frac{\partial\Phi}{\partial x} \quad (3.21)$$

$$\overline{w\phi} = -K_\phi \frac{\partial\Phi}{\partial z} \quad (3.22)$$

The exchange coefficient ( $K_\phi$ ) for a passive additive is called eddy diffusivity and can be estimated by the product of a turbulent length ( $l$ ) and velocity ( $u$ ) scale. Thus, combining equations (3.20), (3.21), and (3.22) yields equation (3.23).

$$\varepsilon_n = u \bullet l \left[ \left( \frac{\partial\Phi}{\partial x} \right)^2 + \left( \frac{\partial\Phi}{\partial z} \right)^2 \right] \quad (3.23)$$

Equation (3.23) provides a means of calculating the rate of reduction of inhomogeneity in the refractive index field using the gradients of the potential refractive index field derived from TASS output. For the C-130, the core radius (6 m) is chosen as the scale length ( $l$ ), and the average velocity at the core wall ( $8 \text{ m sec}^{-1}$ ) is chosen as the

velocity scale ( $u$ ). Equations (3.18) and (3.23) can now be combined to form equation (3.24), which predicts refractive index structure constant for wakes of aircraft based on TASS output.

$$C_n^2 \approx a^2 \epsilon^{-1/3} u \cdot l \left[ \left( \frac{\partial \Phi}{\partial x} \right)^2 + \left( \frac{\partial \Phi}{\partial z} \right)^2 \right] \quad (3.24)$$

Figure 3–13 shows the refractive index structure constant field for the C-130 as computed from equation (3.24). The scaling velocity is  $3.9 \text{ m sec}^{-1}$ , and the scaling length is 3.5 meters, as described in equation (3.15). With  $C_n^2$  determined, equation (3.17) can be evaluated for the radar volume reflectivity,  $\eta$ . Since  $\eta$  is weakly dependent on the radar wavelength, the radar volume reflectivity is almost numerically the same as  $C_n^2$  in dB.

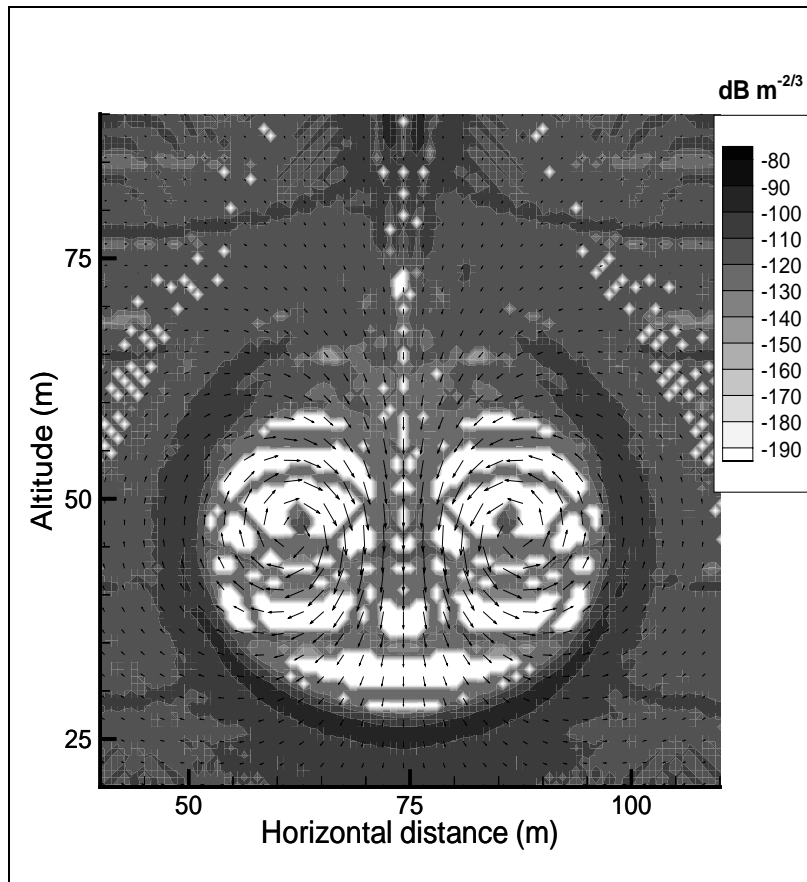


Figure 3–13. Refractive index structure constant for the C-130 at 30 sec after rollup.

#### 4.0 RADAR REFLECTIVITY MODEL FOR FOG

TASS generates the aircraft wake in a fog layer defined by a vertical distribution of bulk, or total liquid water. This leads to an assumption in the wake vortex radar reflectivity factor model, as described in the following discussion.

Liquid water in fog is distributed according to a fog drop size distribution,  $N[D]$ . Equation (4.1) is the definition for radar reflectivity factor in terms of the fog drop size distribution and the drop diameter.

$$Z = \int_{D_{\min}}^{D_{\max}} N[D]D^6 dD \quad (4.1)$$

where  $N[D] \equiv$  Fog drop size distribution; and  $D \equiv$  Fog drop diameter.

The ideal method for predicting radar reflectivity factor,  $Z$ , on an output grid in fog would use a vertical sounding of drop size distribution as input and would provide output of drop size distribution at each grid point. However, TASS does not currently include the cloud physics necessary to determine quantitatively if collision and coalescence in the flow of the wake are altering the initial atmospheric drop size distribution. TASS modelers speculate that the time scales required for the growth of drops is large compared to the life of the wake (Proctor, 1996), since cloud drop size to raindrop size growth by collision and coalescence occurs over time scales as small as 20 minutes in the atmosphere (Rogers, 1989). Lifetimes of wake vortices are an order of magnitude smaller than 20 minutes; yet, the effect of turbulence on coalescence of smaller drops into larger drops is not well understood (Rogers, 1989). If collision and coalescence are producing larger drops, then equation (4.1) indicates that predictions of radar reflectivity factor from TASS liquid water content data will underestimate actual values.

The radar reflectivity factor can be calculated by empirical relationships between  $Z$  and bulk liquid water as shown in equation (4.2).

$$Z \approx aM^b \quad (4.2)$$

where  $M \equiv$  bulk liquid water content ( $\text{gm m}^{-3}$ ) and where  $a$  and  $b$  are empirical constants.

Initially, the only available values for a and b in equation (4.2) resulted from cloud observations (Atlas, 1954). Efforts have been made in the development of the fog model to find values of a and b that describe the fog layer which was provided as TASS input.

#### 4.1 Atlas Radar Reflectivity Factor Model

The liquid water content field in Figure 2–6 from Section 2 can be converted to radar reflectivity factor by the empirical relationship in equation (4.3) (Atlas, 1954).

$$Z = 0.048M^2 \quad (4.3)$$

where  $Z \equiv$  radar reflectivity factor ( $\text{mm}^6 \text{m}^{-3}$ ); and  $M \equiv$  liquid water content ( $\text{gm m}^{-3}$ ).

Figure 4–1 is a plot of equation (4.3) evaluated using the liquid water content from Figure 2–6. The data indicates that radar reflectivity factors as high as -20 dBZ exists at 100 meters above the surface in the averaged VAFB fog layer.

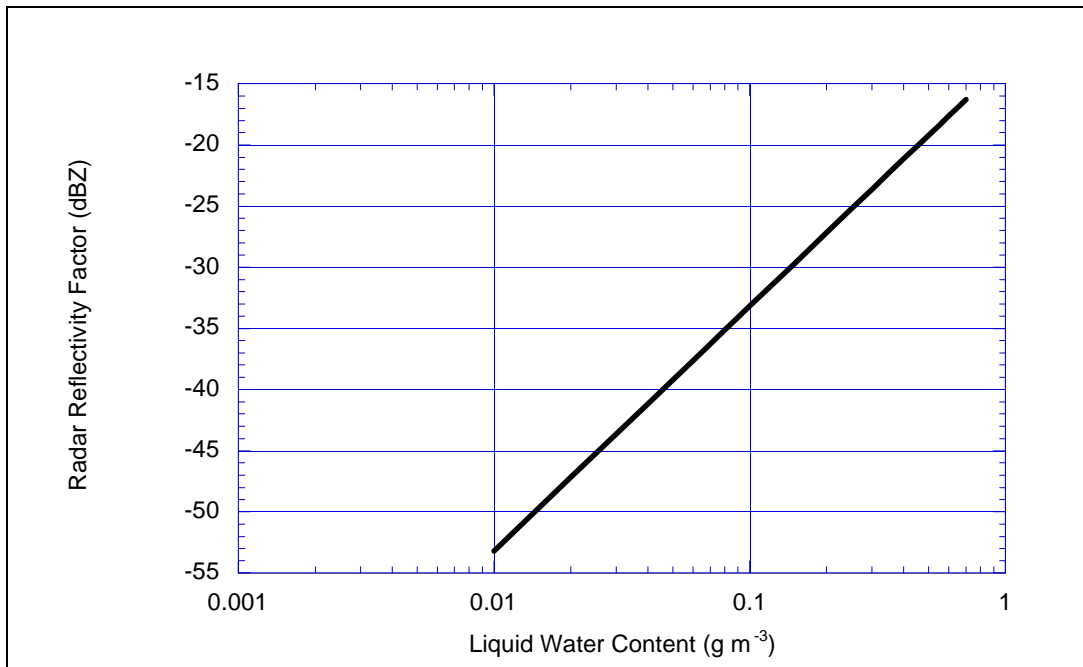


Figure 4–1. Radar reflectivity factor as calculated from the relationship by Atlas.  
( $Z = 0.048 M^2$ )

Figure 4–2 applies equation (4.3) to the TASS liquid water content field in Figure 2–9. Again, the wake is released in the VAFB fog layer described in Section 2.

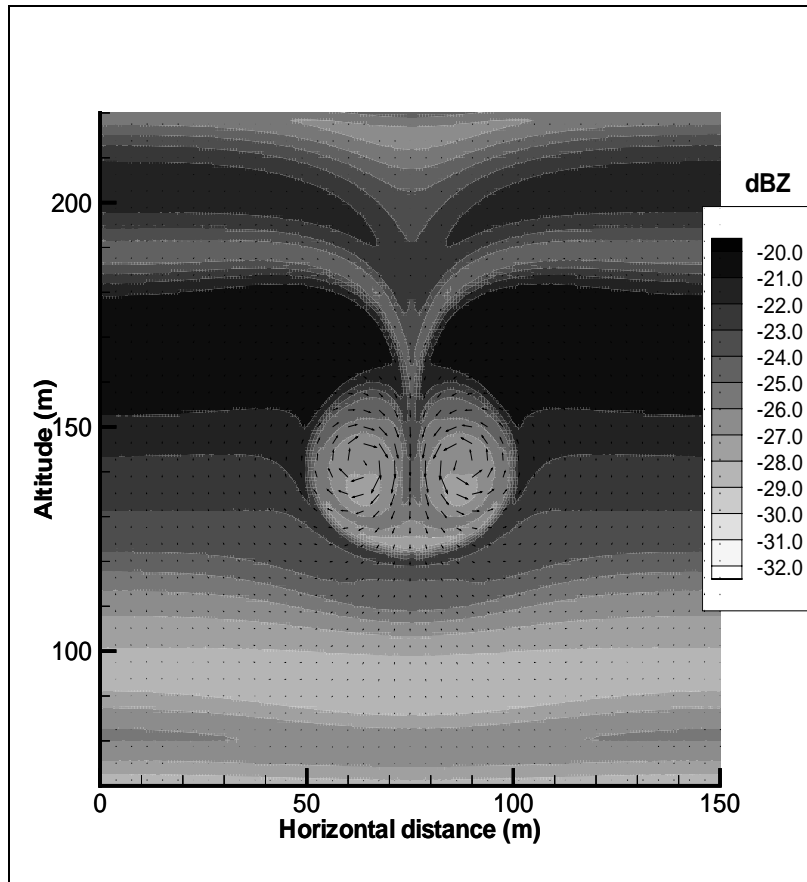


Figure 4–2. Radar reflectivity factor in the wake of a C-130, 30 seconds after rollup in the VAFB fog layer using the Atlas empirical relationship.

#### 4.2 de Wolf Radar Reflectivity Factor Model

An empirical relationship—equation (4.4)—that is specific to the VAFB fog layer was developed by David de Wolf (de Wolf, 1997):

$$Z = 0.0243M^{1.494} \tag{4.4}$$

where  $Z \equiv$  radar reflectivity factor ( $\text{mm}^6 \text{m}^{-3}$ ); and  $M \equiv$  liquid water content ( $\text{gm m}^{-3}$ ).

Figure 4–3 depicts radar reflectivity factor in the wake of a C-130 at 30 seconds after rollup in the VAFB fog layer using the TASS output of Figure 2–9 and the de Wolf relationship in equation (4.4).

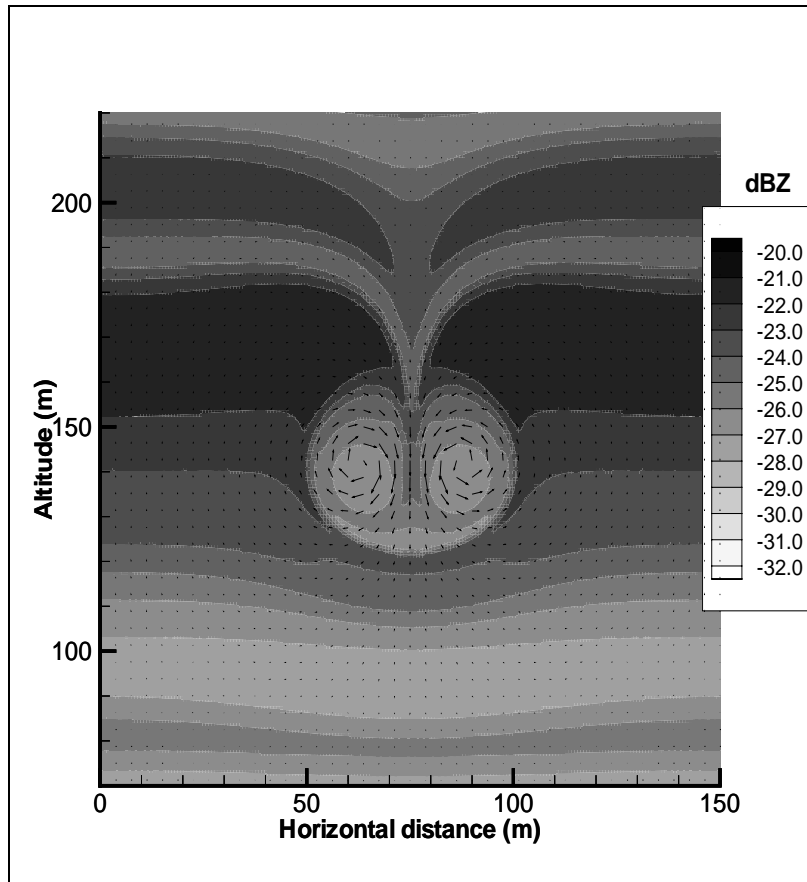


Figure 4–3. Radar reflectivity in the wake of a C-130 at 30 seconds after rollup in the VAFB fog layer using the de Wolf empirical relationship between Z and M.

#### 4.3 Comparison of Models and Assumptions

Figure 4–4 (Marshall, de Wolf, and Kontogeorgakis, 1996) compares equation (4.3) (empirical) to equation (4.1) (analytical) for predicting radar reflectivity factor from TASS output in the VAFB fog at each 10 meters in the vertical in the VAFB fog layer.

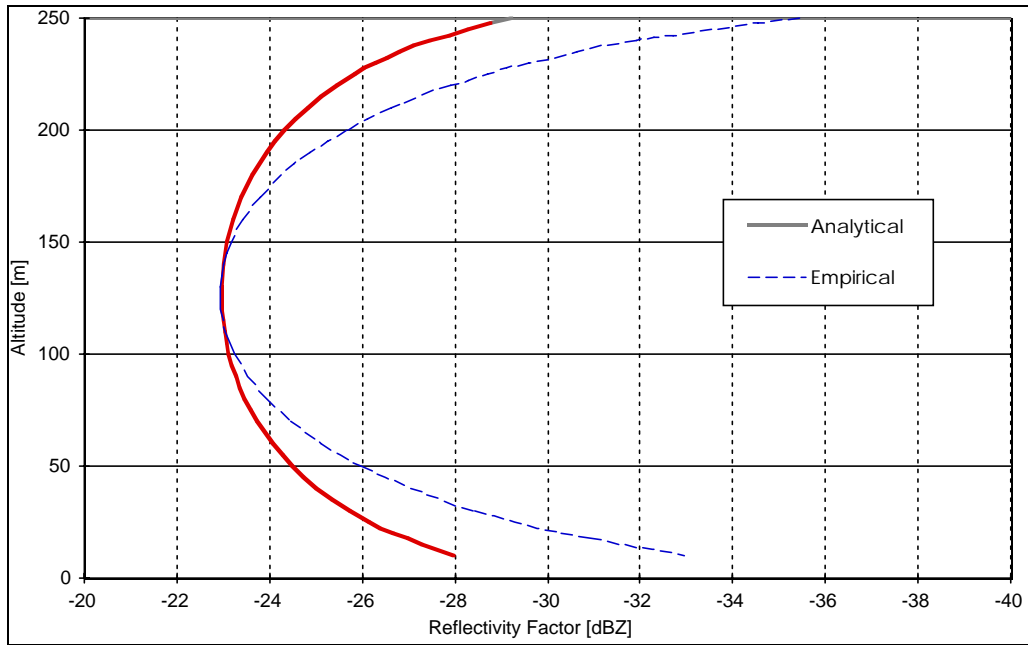


Figure 4–4. Comparison between the Atlas empirical relationship and the analytical relationship for radar reflectivity factor in the VAFB fog layer.

Figure 4–4 indicates that the Atlas empirical relationship underestimates radar reflectivity factor in areas of the VAFB fog layer where the liquid water content is lowest. At 10 meters above the surface, the empirical relationship underestimates the radar reflectivity factor by 5 dB.

Figure 4–5 provides a comparison of radar reflectivity factors calculated from the Atlas and de Wolf relationships. The figure shows that in the VAFB fog layer where liquid water content is less than  $0.05 \text{ g m}^{-3}$ , radar reflectivity factor will be at least 3 dB higher than predicted by the Atlas relationships. A radar design evaluated using the Atlas relationship would have a higher signal-to-noise ratio than predicted analytically in environments with low liquid water content.

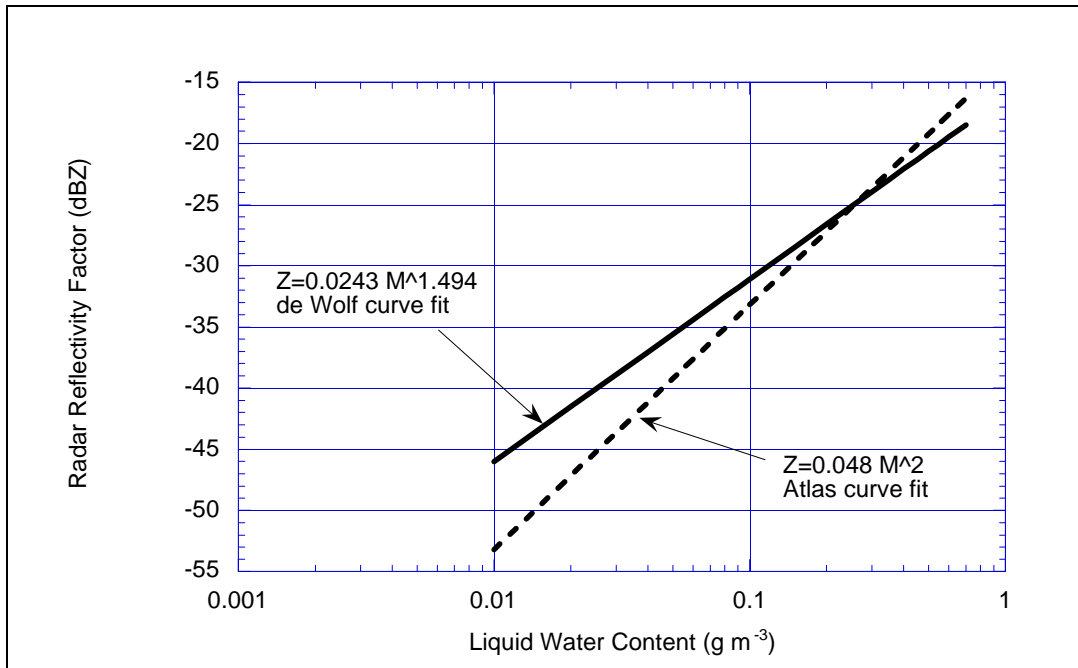


Figure 4–5. Comparison between the de Wolf and Atlas empirical relationship between liquid water content and radar reflectivity factor.

A comparison of Figures 4–2 and 4–3 is shown in Figure 4–6 where the difference in dB between the two wake targets is displayed with the Atlas relationship as the reference. Figure 4–6 indicates that in this dense fog and at this time (30 sec after rollup) there is less than a 1.0 dB increase in Z associated with the individual vortices when applying the empirical relationship between Z and M that is specific to the fog layer. As the wake descends into areas with lower liquid water content, this difference should increase.

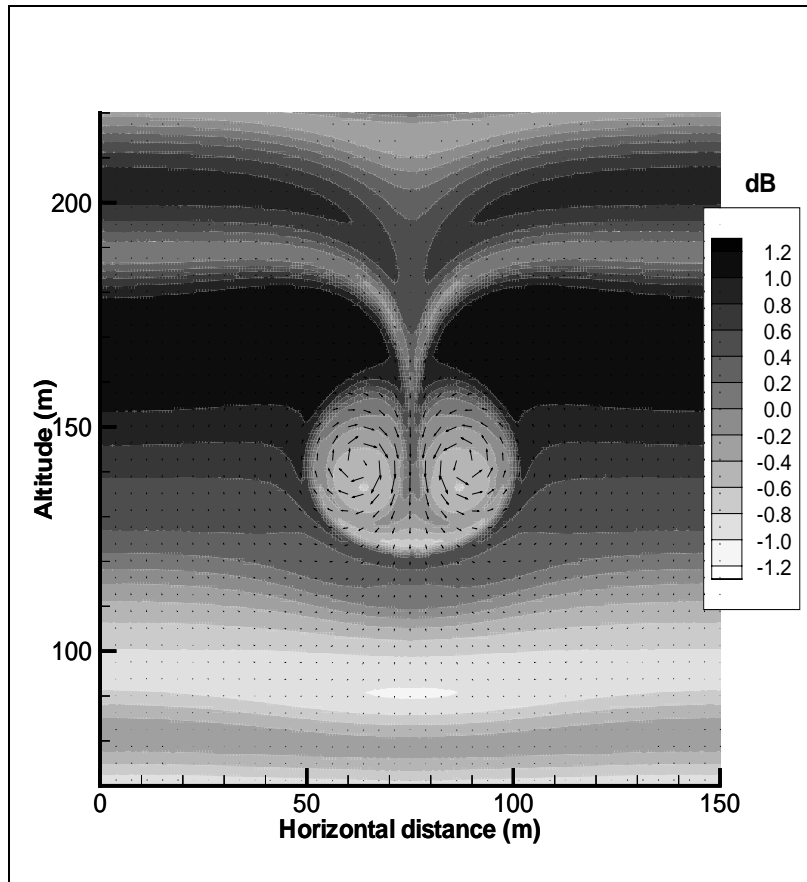


Figure 4-6. Figure 4-2 minus Figure 4-3 in dB.

#### 4.4 Volume Reflectivity in Fog

If the fog drops are small compared to the radar wavelength, equation (4.5) describes the relationship between radar volume reflectivity and radar reflectivity factor (Battan, 1973). Fog drops rarely exceed 50 microns in radius and are small compared to millimeter wavelengths.

$$\eta = \frac{\pi^5 |K|^2}{\lambda^4} Z \quad (4.5)$$

Figure 4-7 shows equation (4.5) for a 35 GHz radar operating in the VAFB fog and using the de Wolf relationship for Z.

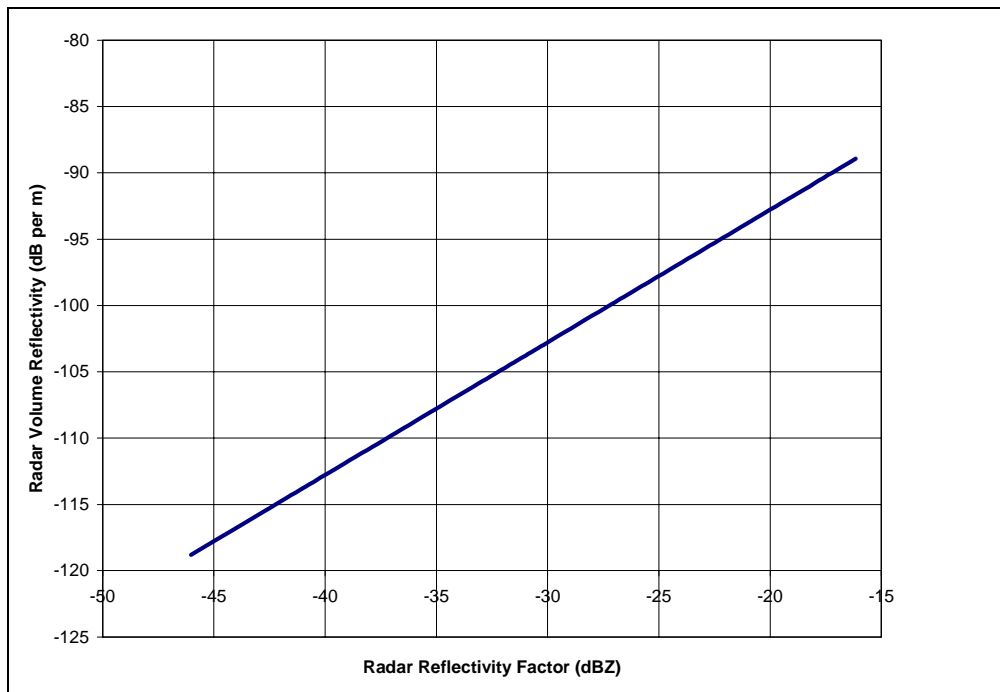


Figure 4–7. Radar volume reflectivity calculated from equation (4.5) and the radar reflectivity factor,  $Z$ , from the de Wolf empirical relationship.

## 5.0 CONCLUSIONS

This report documents the development of radar reflectivity models for the wakes of aircraft flying in clear air and fog. Radar volume reflectivity in clear air is assumed to be due to half radar wavelength inhomogeneities in the temperature, pressure and humidity fields produced by turbulence. Radar reflectivity factor in fog is assumed to be produced by backscattering from small spherical fog drops. Both the clear air and fog reflectivity models require as input the mean wind and thermodynamic variables from a 2D large eddy simulation wake vortex model.

The results of the clear air radar reflectivity model indicate that the small scale inhomogeneities in potential refractive index are more dependent on humidity gradients than perturbations in the temperature and pressure fields. The largest gradients in the potential refractive index field are associated with the boundary of the descending volume of air containing the two vortices, which has the highest values of refractive index structure constant and radar volume reflectivity. For the wake of the C-130 used as an example in this report, this highly reflective semicircle contains values of refractive index structure constant between -90 and -110 dB m<sup>-2/3</sup> and is only 5 meters wide. Doppler velocities in this ring of high reflectivity are more associated with the descent rate of the vortices than the hazardous higher tangential winds near the vortex core walls. Values of refractive index structure constant adjacent to the individual vortex core walls vary between -120 and -180 dB m<sup>-2/3</sup>. The atmosphere this wake is generated in is relatively humid and reflectivity values may vary in other atmospheres with more or less water vapor.

Modeling of clear air reflectivity in wake vortices also assumes that the half radar wavelength turbulent eddies are in the inertial subrange of the turbulent kinetic energy wave number spectrum. Although equations relating radar volume reflectivity to refractive index structure constant may be found in the literature for the dissipation range, the resulting reflectivity is too low to be detected by a commercially practical radar. The predictions of maximum radar frequency based on the requirement that the half radar wavelength turbulent eddies be in the inertial subrange of turbulence indicate that the maximum radar frequency is higher in the individual vortices where the smaller scales of turbulence exist. For the wake of the C-130, a 10 GHz radar should be able to detect the

highly reflective ring as well as the individual vortices. A 20 GHz radar should not be effective in measuring the Doppler velocities in the highly reflective ring; however, a 20 GHz radar should be able to detect the areas immediately adjacent to the individual vortex core walls.

Modeling of radar reflectivity factor in the wakes of aircraft flying in fog requires a high resolution description of the distribution of liquid water content in the wake and the choice of an appropriate relationship between radar reflectivity factor,  $Z$ , and liquid water content,  $M$ . Comparisons between  $Z$  values calculated from a 40 year old  $Z/M$  relationship and a  $Z/M$  relationship calculated from a knowledge of the drop size distribution in the VAFB fog indicate small differences in predicted  $Z$  that have minor impact upon the design of a pulsed radar, except at the lower values of  $M$ . As future models for  $Z$  are calculated for wakes released in thick, moderate, and light fog, it will be important to develop specific  $Z/M$  relationships for each fog layer based on a the fog drop size distribution.

## REFERENCES

- Atlas, D., 1954. The Estimation of Cloud Parameters by Radar. *Journal of Meteorology*, **11**.
- Battan, L. J., 1973. *Radar Observation of the Atmosphere*. The University of Chicago Press.
- Brown, R. A., 1991. *Fluid Mechanics of the Atmosphere*. Academic Press.
- Cohn, S. A., 1994. Investigations of the Wavelength Dependence of Radar Backscatter From Atmospheric Turbulence. *Journal of Atmospheric and Oceanic Technology*, **11**: 2, pp. 225-238.
- Cohn, S. A., 1991. Near Simultaneous Observations of Clear Air Turbulence with UHF, L-band, and X-band Radars at Millstone Hill. 25th International Conference on Radar Meteorology, Paris, France.
- de Wolf, D. A., C. Kontogeorgakis, and R. E. Marshall, 1997. Reflectivity and Attenuation at Millimeter to Infrared Wavelengths for Fogs at Five Locations. *Proceedings of the 28<sup>th</sup> Conference on Radar Meteorology*, AMS.
- Doviak, R. J. and D. S. Zrnic, 1984. *Doppler Radar and Weather Observations*. Academic Press, Inc.
- Hess, S. L., 1979. *Introduction to Theoretical Meteorology*. Robert E. Krieger Publishing Co., Huntington, NY.
- Hill, R. J., 1978. Spectra of Fluctuations in Refractivity, Temperature, Humidity, and the Temperature-Humidity Cospectrum in the Inertial and Dissipative Ranges. *Radio Science*, **13**, pp. 953-961.
- Hinton, D. A., 1995. Aircraft Vortex Spacing System (AVOSS) Conceptual Design. NASA Technical Memorandum 110184, Langley Research Center.
- Iribarne, J. V. and W. L. Godson, 1981. *Atmospheric Thermodynamics*. D. Reidel Publishing Co., Dordrecht, Holland.
- Marshall, R. E., W. A. Davis, and E. Caswell, 1997. Wake Vortex Ka-band Radar Technology. Technical Memorandum RTI/4500/041-05S-R, Research Triangle Institute.
- Marshall, R. E., D. A. de Wolf, and C. Kontogeorgakis, 1996. Visibility and Radar Reflectivity Factor in Fog and Haze. Technical Memorandum RTI/4500/041-06S, Research Triangle Institute.

- Marshall, R. E., and A. S. Mudukutore, 1996. Wake Vortex Radar Performance Studies and Simulated Detection of Wake Vortices by a Ka-band Radar in Fog. Technical Report RTI/4500/053-01F, Research Triangle Institute.
- Marshall, R. E., W. Scales, and T. Myers, 1996. Spatio-temporal Characteristics of Radar Reflectivity in Wingtip Generated Wake Vortices. Technical Memorandum RTI/4500/041-07S, Research Triangle Institute.
- Nieuwstadt, F. T. M., and H. van Dop, 1982. Atmospheric Turbulence and Air Pollution Modeling. D. Reidel Publishing Co., Dordrecht, Holland.
- Ottersten, Hans, 1969. Atmospheric Structure and Radar Backscattering in Clear Air. Radio Science, December, pp. 1179-1193.
- Pasquill, F., and F. B. Smith, 1983. Atmospheric Diffusion. Halstead Press.
- Proctor, F. H., 1987. The Terminal Area Simulation System. NASA Contractor Report 4046, DOT/FAA/PM-86/50.
- Proctor, F. H., 1996. personal communication.
- Rogers, R. R., and M. K. Yau, 1989. A Short Course in Cloud Physics. Pergamon Press.
- Sorbjan, Z., 1989. Structure of the Atmospheric Boundary Layer. Prentice Hall.
- Tatarski, V. I., 1961. Wave Propagation in a Turbulent Medium. McGraw Hill.
- Tennekes, H., and J. L. Lumley, 1987. A First Course in Turbulence. The MIT Press, pp. 19-20.
- Trout, D., and H. A. Panofsky, 1969. Energy Dissipation Near the Tropopause. Tellus, **21**:3.
- Wallace, J. M., and P. V. Hobbs, 1977. Atmospheric Science, An Introductory Survey. Academic Press, Inc.
- Zak, J. A., 1994. Drop Size Distributions and Related Properties of Fog for Five Locations Measured from Aircraft. NASA Contractor Report 4585, DOT/FAA/CT-94/02.

## GLOSSARY

2D  $\equiv$  two dimensional

AVOSS  $\equiv$  Aircraft Vortex Separation System

$a^2 \approx 3.6$

B  $\equiv$  noise bandwidth

c  $\equiv$  speed of light =  $3 \times 10^8$  m sec<sup>-1</sup>

$C_n^2$   $\equiv$  refractive index structure constant

$c_p$   $\equiv$  specific heat at constant pressure =  $1004$  J deg<sup>-1</sup> kg<sup>-1</sup>

D  $\equiv$  diameter of fog drops

d  $\equiv$  diameter of turbulent eddy

dB  $\equiv$  decibel

dBZ  $\equiv 10 \log (Z)$

e  $\equiv$  partial pressure due to water vapor

$\varepsilon$   $\equiv$  turbulent kinetic energy dissipation rate

$\varepsilon_N$   $\equiv$  rate of reduction of inhomogeneity in the refractive index field

$e_o$   $\equiv$  potential water vapor pressure

$\varepsilon_r$   $\equiv$  relative permittivity of the atmosphere

$e_s$   $\equiv$  saturation vapor pressure

$\phi$   $\equiv$  instantaneous potential refractive index

$\phi$   $\equiv$  fluctuating potential refractive index

$\Phi$   $\equiv$  mean potential refractive index

G  $\equiv$  antenna gain

GHz  $\equiv 10^9$  Hz

gm  $\equiv$  gram

$\eta$   $\equiv$  radar volume reflectivity

I  $\equiv$  size of the largest energy-containing eddy

k  $\equiv$  Boltzman's constant =  $1.38 \times 10^{-23}$  J °K<sup>-1</sup>

$|K|^2$   $\equiv$  dielectric factor of hydrometeors

$^{\circ}\text{K} \equiv$  degrees Kelvin  
 $K_{\phi} \equiv$  eddy diffusivity  
 $\text{kg} \equiv$  kilogram  
 $K_h \equiv$  exchange coefficient for heat  
 $K_m \equiv$  eddy viscosity  
 $\lambda \equiv$  wavelength  
 $\lambda_K \equiv$  Kolmogorov microscale  
 $L_s \equiv$  radar system loss  
 $\lambda_T \equiv$  Taylor microscale  
 $M \equiv$  bulk liquid water  
 $\text{m} \equiv$  meter  
 $\text{mb} \equiv$  millibar  
 $\nu \equiv$  kinematic viscosity of the atmosphere  
 $N \equiv$  radio refractivity  
 $n \equiv$  refractive index of the atmosphere  
 $N[D] \equiv$  drop size distribution  
 $p \equiv$  total atmospheric pressure  
 $\text{Pa} \equiv$  Pascals  
 $P_o \equiv$  reference pressure = 1000 mb  
 $P_t \equiv$  peak transmitter power  
 $\theta \equiv$  3 dB antenna beamwidth  
 $\theta \equiv$  potential temperature  
 $R \equiv$  radar range  
 $\rho_d \equiv$  density of dry air  
 $R_d \equiv$  dry air gas constant =  $287 \text{ J deg}^{-1} \text{ kg}^{-1}$   
 $R_{\lambda T} \equiv$  microscale Reynolds number  
 $\rho_v \equiv$  absolute humidity  
 $S/N \equiv$  signal-to-noise ratio  
 $\tau \equiv$  transmitter pulse width

$T$   $\equiv$  atmospheric temperature  
 $TASS$   $\equiv$  Terminal Area Simulation System  
 $TKE$   $\equiv$  turbulent kinetic energy  
 $T_s$   $\equiv$  radar system noise temperature  
 $u$   $\equiv$  instantaneous horizontal component of the wind  
 $U$   $\equiv$  mean horizontal component of the wind  
 $u$   $\equiv$  fluctuating horizontal component of the wind  
 $u$   $\equiv$  velocity of largest energy containing eddy  
 $u^*$   $\equiv$  friction velocity  
 $VAFB$   $\equiv$  Vandenberg, AFB, CA  
 $w$   $\equiv$  fluctuating vertical component of the wind  
 $w$   $\equiv$  instantaneous vertical component of the wind  
 $W$   $\equiv$  mean vertical component of the wind  
 $w$   $\equiv$  water vapor mixing ratio  
 $w_s$   $\equiv$  saturation water vapor mixing ratio  
 $Z$   $\equiv$  radar reflectivity factor

REPORT DOCUMENTATION PAGE			Form Approved OMB No. 0704-0188	
Public reporting burden for this collection of information is estimated to average 1 hour per response, including the time for reviewing instructions, searching existing data sources, gathering and maintaining the data needed, and completing and reviewing the collection of information. Send comments regarding this burden estimate or any other aspect of this collection of information, including suggestions for reducing this burden, to Washington Headquarters Services, Directorate for Information Operations and Reports, 1215 Jefferson Davis Highway, Suite 1204, Arlington, VA 22202-4302, and to the Office of Management and Budget, Paperwork Reduction Project (0704-0188), Washington, DC 20503.				
1. AGENCY USE ONLY (Leave blank)		2. REPORT DATE December 1997		3. REPORT TYPE AND DATES COVERED Contractor Report
4. TITLE AND SUBTITLE Radar Reflectivity in Wingtip-Generated Wake Vortices			5. FUNDING NUMBERS C NAS1-18925 TA 55 WU 538-04-11-15	
6. AUTHOR(S) Robert E. Marshall, Ashok Mudukutore, and Vicki L. H. Wissel				
7. PERFORMING ORGANIZATION NAME(S) AND ADDRESS(ES) Center for Aerospace Technology, Research Triangle Institute, Hampton, VA			8. PERFORMING ORGANIZATION REPORT NUMBER RTI/4500/055-02F	
9. SPONSORING/MONITORING AGENCY NAME(S) AND ADDRESS(ES) National Aeronautics and Space Administration NASA Langley Research Center Hampton, VA 23681-2199			10. SPONSORING/MONITORING AGENCY REPORT NUMBER NASA/CR-97-206259	
11. SUPPLEMENTARY NOTES Langley Contract Monitor: Anne I. Mackenzie, Langley Technical Task Monitor: Robert T. Neece				
12a. DISTRIBUTION/AVAILABILITY STATEMENT Unclassified-Unlimited Subject Category 33                      Distribution: Standard Availability: NASA CASI (301) 621-0390			12b. DISTRIBUTION CODE	
13. ABSTRACT (Maximum 200 words) This report documents new predictive models of radar reflectivity, with meter-scale resolution, for aircraft wakes in clear air and fog. The models result from a radar design program to locate and quantify wake vortices from commercial aircraft in support of the NASA Aircraft Vortex Spacing System (AVOSS). The radar reflectivity model for clear air assumes: 1) turbulent eddies in the wake produce small discontinuities in radar refractive index; and 2) these turbulent eddies are in the "inertial subrange" of turbulence. From these assumptions, the maximum radar frequency for detecting a particular aircraft wake, as well as the refractive index structure constant and radar volume reflectivity in the wake can be obtained from the NASA Terminal Area Simulation System (TASS) output. For fog conditions, an empirical relationship is used to calculate radar reflectivity factor from TASS output of bulk liquid water. Currently, two models exist: 1) Atlas—based on observations of liquid water and radar reflectivity factor in clouds; and 2) de Wolf—specifically tailored to a specific measured dataset (1992 Vandenberg Air Force Base).				
14. SUBJECT TERMS Wake Vortex, Doppler Radar, Radar Meteorology, Reflectivity, Aircraft Safety, Terminal Area Productivity, AVOSS, Bragg Scattering			15. NUMBER OF PAGES 57	
			16. PRICE CODE A04	
17. SECURITY CLASSIFICATION OF REPORT Unclassified	18. SECURITY CLASSIFICATION OF THIS PAGE Unclassified	19. SECURITY CLASSIFICATION OF ABSTRACT Unclassified	20. LIMITATION OF ABSTRACT	